Catena 194 (2020) 104640

Contents lists available at ScienceDirect

Catena

journal homepage: www.elsevier.com/locate/catena

A mineralogical and geochemical investigation of modern aeolian sands near Tonopah, Nevada: Sources and environmental implications

Traister Oglesbee[a,b], Claire L. McLeod[a], Caleb Chappell[a,b], Jordan Vest[a], Dan Sturmer[c], Mark P.S. Krekeler[a,b,*]

[a] Department of Geology and Environmental Earth Science, Shideler Hall, Miami University, Oxford, OH 45056, United States
[b] Department of Mathematical and Physical Sciences, Miami University Regionals, Hamilton, OH 45011, United States
[c] Department of Geology, University of Cincinnati, Cincinnati, OH 45221, United States

ARTICLE INFO

Keywords:
Sand dune
Geochemistry
Mineralogy
Tonopah, Nevada
Geogenic background
Environmental reference

ABSTRACT

The mineralogical and geochemical composition of sands across arid to semi-arid landscapes can be used to evaluate the nature of their source lithologies. Once these characteristics are established, these sands have the potential to be implemented as background reference materials in environmentally-focused studies (e.g., mine waste pollution). Tonopah, Nevada is an economically disadvantaged town with a long history of silver mining. Tonopah and surrounding areas with similar histories are also examples of significantly understudied regions with respect to several environmental concerns.

Sands sampled in this study are part of a star-shaped dune system ~15 km north of Tonopah. They are medium-grained and are very well sorted: arithmetic mean grain size from 263 to 335 μm. From Quartz – Feldspar – Lithic (QFL) classification the sands are feldspathic litharenites to weakly litharenitic. Powder X-ray diffraction and polarized light microscopy observations identify quartz, ordered calcian albite, and sanidine as the dominant minerals with rarer calcite, magnesian calcite, and amphibole. Scanning electron microscopy indicates grains have a range of textural maturity, with rhyolitic and basaltic lithic grains present. From bulk elemental chemistry, sands are geochemically akin to that of Earth's bulk upper continental crust, are quartz-rich, formed in arid to semi-arid climates, and were derived from a felsic igneous province (or provinces).

The origin of these sands is further investigated by comparing bulk major elemental signatures to the composition of global, regional, and local dune systems, in addition to local and regional bedrock. Regionally, Tonopah sands are compositionally similar to those of the Mojave Desert dune fields (e.g. Cadiz) and distinct from those of the Algodones and Parker dunes of California and Arizona respectively. Consistent with source inferences for the Cadiz, Danby, and Dale lake sands of the Mojave Desert, Tonopah sands are inferred to be derived from chemically evolved provinces. For Tonopah, derivation from the local, Micoene-aged, andesite-dacite-rhyolite suites is inferred.

Through comprehensive characterization of the Tonopah sands a geogenic background composition for the region, and an important reference material for future environmental investigations, has been established.

1. Introduction

Globally, sand dune systems are important ecosystems and common geomorphological features across continental landscapes (e.g., Lancaster, 2013; Hugenholtz et al., 2012). On more local and regional scales, these dynamic systems are integral to sediment transportation and depositional pathways (e.g., Kocurek and Lancaster, 1999; Lancaster et al., 2015) and can therefore be used to investigate the origin (and nature) of particulate matter across arid to semi-arid areas (e.g., Kasper-Zubillaga and Zolezzi-Ruiz, 2007, Fig. 1a).

The state of Nevada (the "Silver State") has a long history of mining with extensive silver (and gold) exploration dating back to 1858 at the Comstock Lode which later developed into the United States' first major silver mine (e.g., Bastin, 1922; USGS, 2014, Perry and Visher, 2015). As of 2017, according to the Nevada Commission on Mineral Resources (NCMR, 2017), 63 major mines across the state are in operation today with a total of 14,118,926 ounces of silver and gold produced in 2017 (for a total value of $7.2 billion). The town of Tonopah, NV (Fig. 1a,b) has existed since *c.* 1900 as a result of the discovery of silver ore. While silver mining operations experienced a minor revival in the 1980s,

* Corresponding author at: Department of Geology and Environmental Earth Science, Shideler Hall, Miami University, Oxford, OH 45056, United States.
E-mail address: krekelmp@miamioh.edu (M.P.S. Krekeler).

https://doi.org/10.1016/j.catena.2020.104640
Received 30 December 2019; Received in revised form 6 April 2020; Accepted 28 April 2020

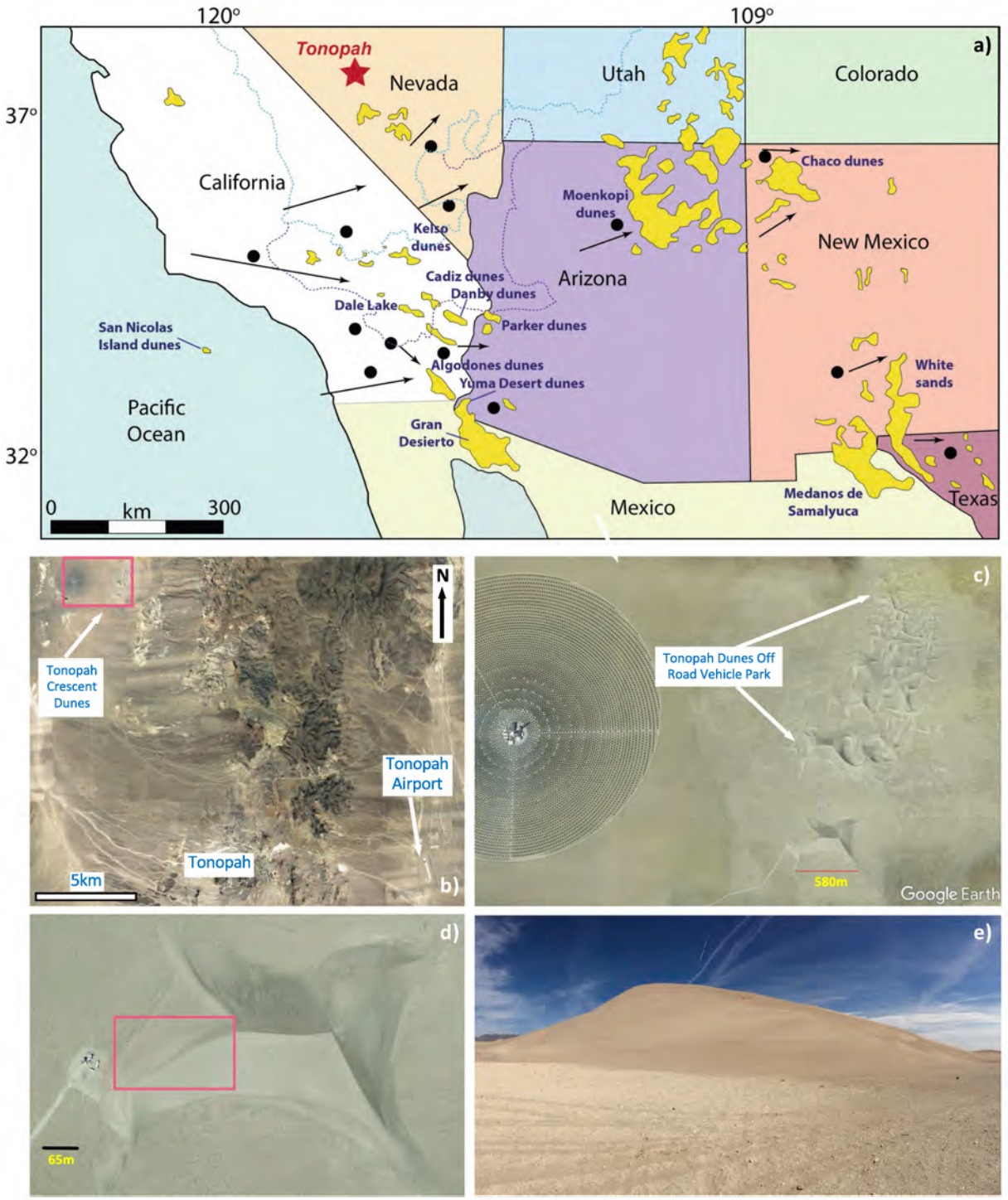

Fig. 1. (a) Location of map of the study area, Tonopah, NV, shown in relation to other studied dune fields of the western US. Arrows summarize drift direction and potential. Solid circles mark location of wind station locations. Map modified from Muhs et al. (2003) and Muhs (2017). Outline of the Great Basin (dashed blue) and Mojave Desert (dashed purple) shown to highlight the location of the field area relative to other well-studied dune fields across the desert region of the western US. Tonopah is located in the Great Basin, in south-central Nevada to the south of the Toiyabe Mountain Range. The star-shaped dune system (known locally as Tonopah Crescent Dunes) which is the focus of this study lies ~15 km to the north–north-west of the town of Tonopah and ~2 km directly east of Crescent Dunes Solar Energy Plant (see panels b, c). An Off-Road Vehicle Park exists to the north of Big Dune which is the specific focus of this study (see panels d, e). (For interpretation of the references to colour in this figure legend, the reader is referred to the web version of this article.)

significant exploration ceased after World War II.

Overall, despite extensive historic and active mining operations, in addition to military installations and nearby preserved lands in central Nevada, environmental investigations of metal pollution are limited. One crucial component of conducting meaningful metal pollution assessments is finding appropriate environmental comparison materials. The large star dune system in the Tonopah Crescent Dunes system represents one such potential reference material. Previous work investigating sand dune sedimentology in Nevada is limited with prior studies focusing on the Winnemucca Dunes in Humboldt County (northwest Nevada *c.* 260 miles north of Tonopah; Pepe, 2014), Silver Peak, in Esmeralda County (south-central Nevada *c.* 35 miles southwest

of Tonopah, Nickling et al., 2002; Walker, 1999; McKenna Neuman et al., 1997) in addition to Nellis Dunes in Clark County (southern Nevada, *c*. 125 miles southeast of Tonopah *c*. 20 miles northeast of Las Vegas; McLaurin et al., 2011; Goossens and Buck, 2010). Most notably, recent work at the Nellis Dune Recreational Area has indicated arsenic as a human exposure concern (Keila et al., 2018; Goossens et al., 2015; Goossens et al., 2012; Soukup et al., 2012). Compared to other areas in the U.S. such as adjacent California, Nevada has had comparatively few investigations of metal pollution whether that pollution originated from mine waste or other sources. There has been some work in the area of atmospheric dispersal of tungsten and cobalt pollution in Fallon, Nevada by Sheppard et al. (2012) and Sheppard et al. (2007) with several studies focusing on mercury derived from mine waste and related activities (Eckley et al., 2011; Custer et al., 2007; Cizdziel et al., 2003; Henny et al., 2002; Engle et al., 2001; Miller et al., 1998; Miller et al.,1996). In addition, several investigations over the last two decades have focused on the origin and impact of multiple metals as pollutants (or recorders of human activity: Sims et al., 2013; Adhikari et al., 2011; Sims, 2010; Yang et al., 2003; Heyvaert et al., 2000). In Nevada specifically, other pollution-oriented studies include that of Donato et al. (2007) who investigated cyanide pollution and Kersting et al. (1999) who investigated plutonium.

Tonopah Crescent Dunes (as they are locally known) are located approximately 15 km to the northwest of Tonopah, approximately 2 km west of the San Antonio Mountains, and approximately 1 km east of the Crescent Dunes Solar energy project (Fig. 1b,c). This sand body may therefore be an appropriate environmental reference material for future metal pollution studies of Tonopah because is it geographically removed from the town by the San Antonio Mountains, but is still part of the same regional geologic setting. In addition to investigating the nature and origin of these sands, and providing a broad environmental reference material for the region (including a geochemical reference for environmental study of metal pollution); a comparative material for climate and geochronology studies across the region (Fig. 1a) will also be provided.

2. Materials and methods

2.1. Samples and setting

Sand samples from the large star dune (the largest dune of the Tonopah Sand dune system), just to the east of the Crescent Dunes Solar energy project solar facility (Fig. 1c-e) were collected in late March of 2019 in plastic bags and vials. Samples were taken approximately 4–5 m from ground level on the leeward side of the dune. At the time of sampling, the dune face was striking N20E. This dune has approximately 25 m of relief, is steep, and is separated from the dune field used as a recreational vehicle park by approximately 1 km (Fig. 1c,d). With respect to prevailing wind direction across the region, wind roses are presented in Supplementary Fig. 1. From Tonopah Airport, the closest wind station for which data is available, the prevailing wind direction is to the north. Regional wind directions are summarized in Fig. 1a for comparison.

2.2. Grain size analysis

Grain size analysis was conducted using 8-inch brass mechanical sieves. Approximately 100 g of sand was used for each analysis. Samples were sieved using a Gibson shaking device using standard sizes between 5.6 mm and 38 μm. Mass retained in each sieve was recorded to the thousandth of a gram. Grain size data was processed with the excel-based program Gradistat.

2.3. Microscopy

Ten slides were prepared commercially by Spectrum Petrographics as round 1-inch diameter epoxy plugs and were polished for electron beam analysis. Samples were analyzed using a Leica polarized light microscope at magnifications from 10X to 50X. Images were captured using a 20MP Leica digital camera.

For scanning electron microscopy (SEM) analysis, selected samples were investigated by mounting grains on carbon sticky tabs on 1 cm diameter aluminum stubs. Selected petrographic slides were further investigated by mounting slides on an aluminum frame and then fixing the slide with carbon tape. Samples were investigated using a Zeiss VP 35 Field emission SEM operated in variable pressure mode with N_2 used as the compensating gas at the Center for Advanced Microscopy and Imaging (CAMI) at Miami University. A Bruker energy dispersive spectrometer (EDS) was used for elemental characterization of individual grains.

2.4. X-ray diffraction

A SPEX 8000 mini mill using a tungsten carbide ball and vial was used to produce powders for X-ray diffraction. Powder X-ray diffraction data was obtained using a Siemens D-5000 housed in the Geology Department at the University of Cincinnati. The instrument uses Cu Kα radiation and scan parameters of 0.02-degree step size over a range of 5–60 degrees 2θ were used.

2.5. X-Ray fluorescence (XRF) and inductively coupled plasma-mass spectrometry (ICP-MS)

Samples were prepared by first milling sands in a SPEX 8000 mini mill using a tungsten carbide ball and vial. Approximately 1.00–1.10 g of powder was used for loss on ignition (LOI) calculations at 950 °C. Sample powders were then prepared by first mixing 0.50 g of sample with 7.75 g of lithium borate bromide flux. Sample powders were them mixed thoroughly by hand for 3 min in a glass vial and the mixed powder was then placed in a platinum crucible and then in a Katamax fused pellet machine. Samples were then cycled to a temperature of 1050 °C over a period of 14:30 including cooling. Melt was then poured at the end of the cycle into a platinum pan to cast the pellet.

X-ray fluorescence analyses were performed using a Rigaku Supermini 200 wavelength-dispersive XRF spectrometer at the University of Cincinnati. Samples were analyzed under vacuum and referenced to internal standards. Data reduction was completed using Rigaku's ZSX software. The Supermini 200 analyzes for elements between fluorine and uranium, and reported data are processed with LOI values. Elements lighter than fluorine were not analyzed.

A subset of samples (one from the start, middle, and end of the sample transect) were sent to the Peter Hooper GeoAnalytical Lab at the University of Washington for bulk trace elemental analysis via ICP-MS. Not all 10 samples were sent for analysis due to associated costs. For trace elements sample preparation, a combined fusion-dissolution procedure was implemented. Samples were fused with $Li_2B_4O_7$ in a 1:1 ratio prior to a sequence of dissolution steps in HNO_3-HF-$HClO_4$ ± H_2O ± H_2O_2. Samples were analyzed using an Agilent 4500 ICP-MS with long-term precision reported at better than 5% (RSD) for the rare earth elements and 10% for the other reported trace elements.

2.6. Reflective spectroscopy

Plastic 100 mm petri dishes were painted with flat black spray paint and allowed to dry for several days. Samples dishes were then filled to a depth of approximately 5 mm in thickness. Samples were measured with an ASD FieldSpec 4 High Resolution spectroradiometer with a five-degree foreoptic attachment at a distance of 10 cm and were illuminated with an ASD Illuminator reflectance lamp with a 70-watt quartz-tungsten-halogen light source in an otherwise dark room. Spectra were measured from 350 to 2500 nm with a 3 nm resolution in the VNIR (350–1000 nm) and an 8 nm resolution in the SWIR (1000–2500 nm).

Table 1
Grain size analysis of sampled sands (1–10).

	SAMPLE TYPE: SEDIMENT NAME:	Bimodal Well Sorted Med. Sand	Unimodal V. Well Sorted Med. Sand	Unimodal Well Sorted Med. Sand	Unimodal V. Well Sorted Med. Sand	Unimodal Well Sorted Med. Sand	Unimodal V. Well Sorted Med. Sand	Unimodal V. Well Sorted Med. Sand	Unimodal Well Sorted Med.Sand	Unimodal V. Well Sorted Med. Sand	Unimodal V. Well Sorted Med. Sand
METHOD OF MOMENTS Arithmetic (αm)	MEAN	289.4	268.1	286.1	267.0	335.0	296.6	282.6	311.6	295.1	262.9
	SORTING	87.43	53.30	78.27	62.85	90.15	61.06	61.84	73.31	70.12	58.67
	SKEWNESS	1.232	0.874	1.170	1.524	0.771	0.884	0.531	0.485	0.799	0.813
	KURTOSIS	4.651	4.753	4.870	8.553	4.298	4.771	4.166	3.152	3.893	4.238
METHOD OF MOMENTS Geometric (αm)	MEAN	276.8	262.1	275.5	259.4	321.6	289.5	274.9	301.9	286.2	255.7
	SORTING	1.324	1.213	1.294	1.248	1.324	1.222	1.247	1.267	1.261	1.244
	SKEWNESS	0.390	0.114	0.283	0.205	−1.214	0.086	−0.226	−0.160	0.108	0.078
	KURTOSIS	3.312	3.659	3.451	4.641	15.64	3.693	3.214	2.938	2.998	3.212
METHOD OF MOMENTS Logarithmic (ϕ)	MEAN	1.853	1.932	1.860	1.947	1.637	1.788	1.863	1.728	1.805	1.967
	SORTING	0.404	0.279	0.372	0.320	0.405	0.289	0.319	0.342	0.334	0.315
	SKEWNESS	−0.390	−0.114	−0.283	−0.205	1.214	−0.086	0.226	0.160	−0.108	−0.078
	KURTOSIS	3.312	3.659	3.451	4.641	15.64	3.693	3.214	2.938	2.998	3.212
FOLK AND WARD METHOD (αm)	MEAN	277.9	262.2	274.0	257.4	325.9	288.0	274.7	303.2	286.5	256.2
	SORTING	1.323	1.218	1.291	1.229	1.289	1.218	1.252	1.278	1.271	1.245
	SKEWNESS	0.193	0.048	0.106	−0.044	0.100	0.062	−0.084	0.006	0.069	0.055
	KURTOSIS	1.134	1.128	1.098	1.249	1.013	1.072	0.975	0.990	1.054	1.024
FOLK AND WARD METHOD (ϕ)	MEAN	1.848	1.931	1.868	1.958	1.618	1.796	1.864	1.722	1.804	1.965
	SORTING	0.404	0.284	0.368	0.298	0.367	0.285	0.324	0.354	0.346	0.316
	SKEWNESS	−0.193	−0.048	−0.106	0.044	−0.100	−0.062	0.084	−0.006	−0.069	−0.055
	KURTOSIS	1.134	1.128	1.098	1.249	1.013	1.072	0.975	0.990	1.054	1.024
FOLK AND WARD METHOD (Description)	MEAN:	Medium Sand	Medium Sand	Medium Sand	Medium Sand	Medium Sand	Medium Sand	Medium Sand	Medium Sand	Medium Sand	Medium Sand
	SORTING:	Well Sorted	Very Well Sorted	Well Sorted	Very Well Sorted	Well Sorted	Very Well Sorted	Very Well Sorted	Well Sorted	Very Well Sorted	Very Well Sorted
	SKEWNESS:	Coarse Skewed	Symmetrical	Coarse Skewed	Symmetrical	Symmetrical	Symmetrical	Symmetrical	Symmetrical	Symmetrical	Symmetrical
	KURTOSIS:	Leptokurtic	Leptokurtic	Mesokurtic	Leptokurtic	Mesokurtic	Mesokurtic	Mesokurtic	Mesokurtic	Mesokurtic	Mesokurtic
MODES	MODE 1 (αm):	275.0	275.0	275.0	275.0	275.0	275.0	275.0	275.0	275.0	231.0
	MODE 2 (αm):	462.5									
	MODE 1 (ϕ):	1.868	1.868	1.868	1.868	1.868	1.868	1.868	1.868	1.868	2.119
	MODE 2 (ϕ):	1.117									
D VALUES	D10 (αm):	199.1	207.7	201.1	195.6	243.7	223.6	202.9	220.5	213.4	192.5
	D50 (αm):	268.6	261.2	271.0	261.4	317.7	286.9	278.6	301.6	281.8	254.5
	D90 (αm):	427.0	341.8	395.5	341.0	461.8	378.1	353.3	412.5	397.0	341.7
	(D90 / D10) (αm):	2.145	1.646	1.966	1.744	1.895	1.691	1.741	1.871	1.860	1.775
	(D90 - D10) (αm):	227.9	134.2	194.3	145.4	218.1	154.5	150.4	192.0	183.6	149.2
	(D75 / D25) (αm):	1.410	1.281	1.393	1.283	1.417	1.293	1.369	1.392	1.356	1.336
	(D75 - D25) (αm):	93.95	64.41	90.71	63.97	113.5	74.90	87.03	100.8	88.12	74.02
	D10 (ϕ):	1.228	1.549	1.338	1.552	1.115	1.403	1.501	1.278	1.333	1.549
	D50 (ϕ):	1.896	1.937	1.883	1.935	1.654	1.801	1.844	1.729	1.827	1.974
	D90 (ϕ):	2.328	2.268	2.314	2.354	2.037	2.161	2.301	2.181	2.228	2.377

(*continued on next page*)

Table 1 (*continued*)

	SAMPLE TYPE:	Bimodal	Unimodal	Unimodal	Unimodal	Unimodal	Unimodal	Unimodal	Unimodal	Unimodal
	SEDIMENT NAME:	Well Sorted Med. Sand	V. Well Sorted Med. Sand	Well Sorted Med. Sand	V. Well Sorted Med. Sand	Well Sorted Med. Sand	V. Well Sorted Med. Sand	Well Sorted Med.Sand	V. Well Sorted Med. Sand	V. Well Sorted Med. Sand
	(D90 / D10) (ϕ):	1.897	1.464	1.729	1.517	1.827	1.540	1.533	1.708	1.672	1.534
	(D90 - D10) (ϕ):	1.101	0.719	0.975	0.802	0.922	0.758	0.800	0.904	0.895	0.828
	(D75 / D25) (ϕ):	1.304	1.202	1.292	1.201	1.366	1.232	1.278	1.322	1.279	1.237
	(D75 - D25) (ϕ):	0.496	0.357	0.478	0.359	0.503	0.371	0.453	0.477	0.439	0.418
CLASSIFICATION	% SAND:	100.0%	100.0%	100.0%	100.0%	99.9%	100.0%	100.0%	100.0%	100.0%	100.0%
	% MUD:	0.0%	0.0%	0.0%	0.0%	0.1%	0.0%	0.0%	0.0%	0.0%	0.0%
	% V COARSE SAND:	0.0%	0.0%	0.0%	0.0%	0.0%	0.0%	0.0%	0.0%	0.0%	0.0%
	% COARSE SAND:	2.6%	0.1%	1.8%	0.9%	4.8%	0.4%	0.2%	0.7%	0.6%	0.1%
	% MEDIUM SAND:	60.0%	59.3%	62.4%	59.8%	84.3%	79.2%	68.2%	78.9%	73.5%	52.9%
	% FINE SAND:	37.2%	40.5%	35.7%	39.1%	10.4%	20.4%	31.6%	20.4%	25.9%	46.9%
	% V FINE SAND:	0.2%	0.1%	0.2%	0.2%	0.4%	0.0%	0.1%	0.0%	0.0%	0.1%
	% V COARSE SILT:	0.0%	0.0%	0.0%	0.0%	0.1%	0.0%	0.0%	0.0%	0.0%	0.0%

White reference calibration with Spectralon™ was performed prior to the commencement of data collection and every 15 min after. Ten spectra were averaged to give a single representative spectrum. Averaged spectra were splice corrected using a splice correct gap value of 1 in order to correct for minor gaps at detector crossover.

3. Results

3.1. Grain size analysis

A summary table of the descriptive statistics and accompanying grain size characteristics for each sample is presented in Table 1. With respect to grain size characteristics the sand samples classify as medium, are very well sorted, with 90% being classified as unimodal. Arithmetic mean values varied from 263 to 335 μm. Sorting values varied from 53.3 to 90.1, skewness from 0.485 to 1.524, and kurtosis from 3.152 to 8.553. Using the descriptive terminology of Folk and Ward, 80% of the samples have symmetrical skewness, 20% have coarse skewness and with respect to kurtosis, 70% are mesokurtic and 3 are leptokutic. The mode for 90% of samples is 275 μm and 231 μm for the remaining 10%. D90/D10 values vary from 1.646 to 2.145. There is a modest positive linear correlation with skewness and increasing grains size with $r^2 = 0.51$ and $p < 0.001$. This tentatively implies that coarser grains exhibit better sorting than finer grains. The arithmetic values reported here, as well as geometric and logarithmic values. All other values or descriptors are reported in Table 1.

3.2. Light microscopy

Supplementary Fig. 2 summarizes these general characteristics as observed under the polarized light microscope at 10× magnification. Grains and lithics are predominantly rounded to subrounded with > 95% of the individual mineral grains being quartzofeldspathic in nature. Fig. 2 highlights the nature of grains which make up the remaining < 5% and the textures commonly observed in the lithic clasts. The remaining < 5% of grains are dominated by mafic phases; biotite, amphibole (Fig. 2 a-c) and rarer clinopyroxenes (Fig. 2c). Minor opaque phases (likely oxides; magnetite ± ilmenite) are also present with rarer accessory zircon also observed and shown included in a plagioclase feldspar in Fig. 2d. Rhyolitic clasts are fine-grained predominantly characterized by quartz and alkali feldspar (Fig. 2e-f). Basaltic clasts range from near-holocrystalline (Fig. 2f-h) to hyalocrystalline (Fig. 2i) but all are characterized by plagioclase feldspar, often displaying lath-like habits, and clinopyroxene (± glass). The presence of these lithics, bimodal with respect to their likely bulk silica contents (rhyolitic vs. basaltic), is entirely consistent with the regional geology where extensive rhyolitic and basaltic flows associated with upper Tertiary (late Oligocene and Miocene-aged) magmatic activity dominate the recent volcanic record (Seibert et al., 2019). Point counting of between 600 and 700 grains per sample sand reveals that 70% of the sands can be classified as feldspathic litharenites, based on the relative proportions of Quartz – Feldspar – Lithic (QFL). This is illustrated in the QFL ternary plot in Fig. 3a. The remaining three samples can be classified as litharenites, although several samples plot near the boundary between these two lithological fields. The proportion of feldspar within the samples varies from 10% to 20% whereas the proportion of lithics varies from 20% to 40% at corresponding variance in the proportion of quartz from 40% to 60%. The feldspathic component includes both plagioclase and alkali feldspar with the lithic components characterized by both mafic and felsic lithologies, which are basaltic and rhyolitic in nature. Also shown in Fig. 3a are the QFL properties of the Winnemucca Dune Complex to the north of Tonopah in NW Nevada, one of the most comprehensively characterized dune fields in the state (Pepe, 2014). As shown, the Winnemucca sands can also be classified as Feldspathic litharenites/litharenites although are notably quartz-poor and lithic-rich in comparison to those sampled at Tonopah. As noted in Pepe (2014)

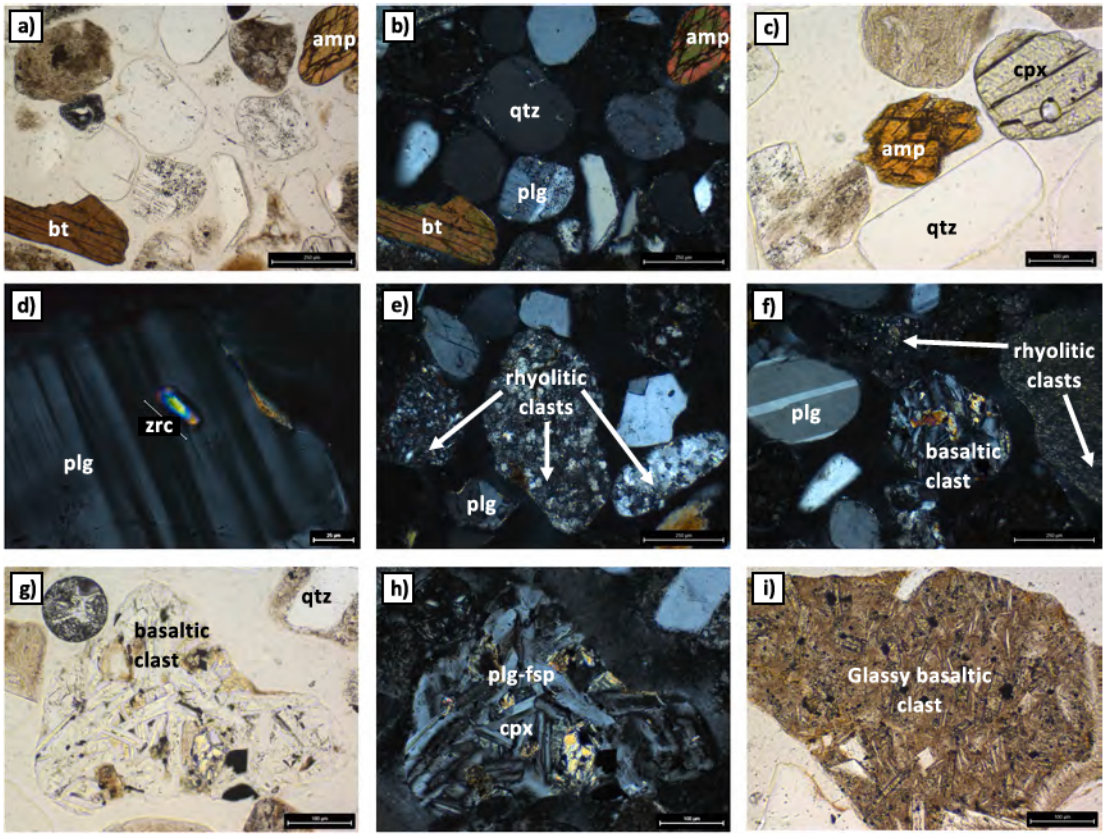

Fig. 2. Summary of sand dune clast mineralogy and mafic phases. (a) Biotite (bt) and Amphibole (amp) grains shown in PPL, (b) in XPL. Plagioclase feldspar (plg) and quartz (qtz) also indicated. (c) Fine-grained felsic igneous clasts (rhyolitic) characterized by qtz and fsp. (d) In XPL, rhyolitic clasts surrounding a basaltic clast characterized by plg and cpx. (e)–(f) PPL and XPL respectively: coarser-grained basaltic lithic clast dominated by plg with < 20%, glass absent. (g) In PPL, fine-grained glassy basaltic clast with microlites of plg, and minor opaque phases (likely oxides). (h) In PPL, demonstrated occurrence of cpx as an individual grain, shown here alongside qtz and amp. (i) Zircon present as an accessory phase within sampled grains, here shown within a plg grain at ~50 in length (in XPL).

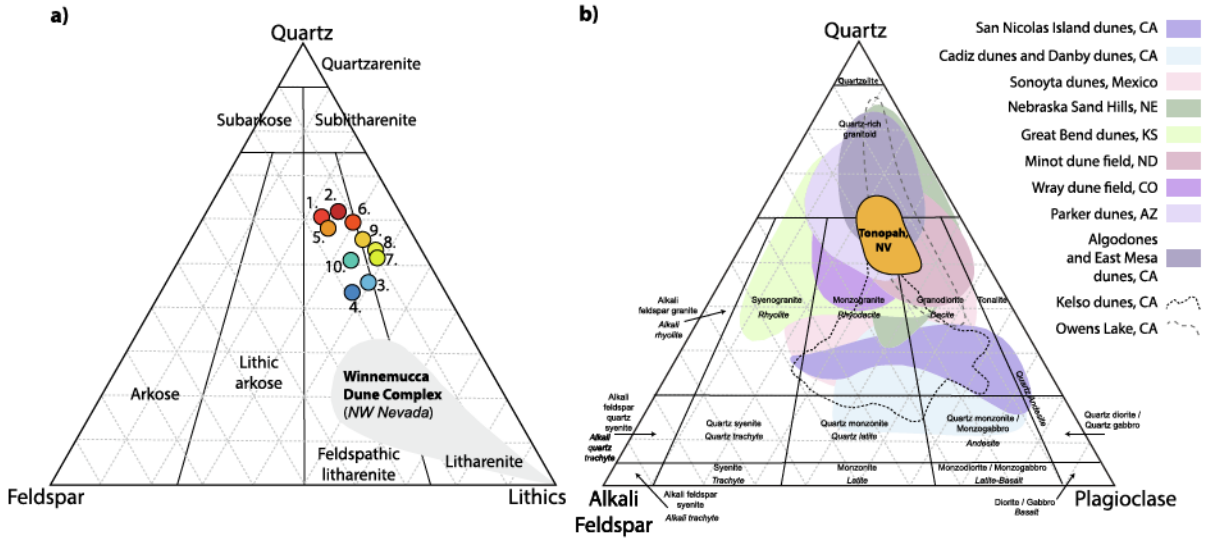

Fig. 3. (a) Ternary Quartz-Feldspar-Lithics diagram classifying the 10 sampled sands as Feldspathic litharenites – litharenites with several samples plotting right at the boundary between the two classifications. The Winnemucca Dune Complex from NW Nevada is the largest dune field in Nevada and lies ~260 miles north of Tonopah. It is one of the few other dune fields from the state of NV that has been previously studied, and is shown here for comparison (data from Pepe, 2014). For discussion see text. (b) Ternary Quartz-Alkali Felspar-Plagioclase diagram comparing the Tonopah Crescent Dune to dune fields across the western US (see Fig. 1 a) for dune field locations). Data from Muhs et al. (2003); Lancaster et al. (2015); Muhs (2017); Muhs et al. (2017). Volcanic and plutonic equivalent rock types from Streckeisen (1976, 1978).

several sampled sands from Winnemucca are 100% composed of lithics. Broadly these sands are dominated by volcaniclastic materials e.g. tuffs and pyroclastic deposits, in addition to metamorphic rock fragments, and are interpreted to reflect derivation from mineralogically and compositionally variable source regions, including metamorphic basement terranes. Metamorphic rock fragments in the Tonopah sands are

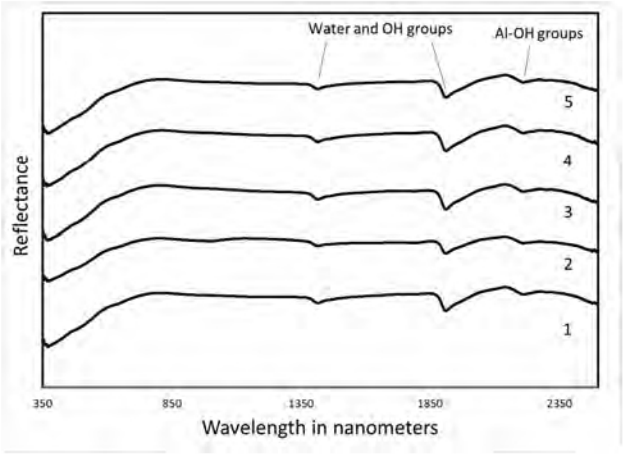

Fig. 4. Representative reflective spectra of samples 1–5 showing major absorptions features at ~1400 nm, ~1900 nm and at 2210 nm. Absorption feature assignments are based on Hunt et al. (1971; 1973).

absent. Fig. 3b compares the relative abundance of Quartz – Alkali Feldspar – Plagioclase (QAP) of the sampled Tonopah sands to local and regional dune fields from across the western US (Fig. 1a). As shown, the mineralogical compositions of dune fields across this region is variable. Regionally, proportions of Q and P are consistently greater than that of A, which is also the case for the Tonopah sands. In comparison, the Tonopah sands are not as mature as the relatively quartz-rich sands of the Algodones and East Mesa dunes of southern California, the Parker dunes of Arizona, or the Sand Hills of Nebraska but are distinctly more mature than the sands of the San Nicolas Island dunes, California and the Wray dune field of Colorado. The nearby Kelso dunes of California (Fig. 1a) are also, predominately, less mature in comparison. The closest sands for comparison to Tonopah in Fig. 3b are the Owens Lake dune fields of eastern California, ~85 miles southwest of Tonopah (Lancaster et al., 2015). The Tonopah sands are also A-poor over a narrow range (~10–20%) but exhibit less Q-P variability.

3.3. Reflective spectroscopy

Reflective spectra of sands show little variation and representative spectra are provided in Fig. 4. All spectra have adsorption features at ~1400 nm, ~1900 nm and ~2210 nm. The absorption features at ~1400 nm and ~1900 nm are associated with water and the presence of OH groups. The adsorption feature at ~2210 nm is associated with Al-OH groups, interpreted as originating from the likely alteration of feldspar minerals and glass. The broad ramp in the visible portion of the spectra is consistent with the bulk Fe content. Feature assignments are based on Hunt et al. (1971; 1973). These spectra are consistent with silicate mineral-rich compositions of the sands.

3.4. Scanning electron microscopy

Representative SEM images of grain mounts of sand samples are presented in Fig. 5 with accompanying EDS spectra. Grains have a range of textural maturity and using the Powers (1953) scale for all SEM images classifications are as follows: 8% very angular, 14% angular, 14% subangular, 20% subrounded, 20% rounded and 25% well rounded. There is a population of lithic grains that tends to be larger than others with common diameters being between 700 and 400 μm, however smaller lithic grains (< 400 μm) are more common. Lithic grains commonly have variable chemical spectra dominated by silica, aluminum, iron, magnesium with lesser amounts of potassium, calcium and manganese. Some lithics however have substantial amounts of calcium and it is possible that these may be grains that are intergrown with soil carbonate. Fe-Ti oxides, which are interpreted as ilmenite, are common in lithic grains and vary in average diameter from approximately 20 to 250 μm. Zircon is also observed as a common inclusion in lithic grains and zircons observed are commonly 30–50 μm in diameter as observed or exposed in the grains. This is consistent with observations via polarized light microscopy (Fig. 2d). Of particular note, there were no sulfides, silver, electrum flake, or arsenic-bearing minerals observed at scales permitted by either the light microscope or SEM (100 s of μm to the sub-micron).

3.5. Powder X-ray diffraction

Minerals identified by X-ray diffraction in sand samples include quartz, ordered calcian albite, sanidine, calcite, and magnesian calcite (Fig. 6). Minerals were identified using the computer program Jade and PDF cards. Quartz was identified using PDF card # 00-046-1045 using the major reflections and d-values of $d_{(1\ 0\ 1)}$ = 3.3435 Å, $d_{(1\ 0\ 0)}$ = 4.2550 Å, and $d_{(1\ 1\ 2)}$ = 1.8120 Å. Ordered calcian albite was identified using PDF card #00-041-1480 using the major reflections and d-values of $d_{(0\ 0\ 2)}$ = 3.1817 Å, $d_{(\bar{2}\ 0\ 2)}$ = 3.1973 Å, $d_{(\bar{2}\ 0\ 1)}$ = 4.0314 Å, and $d_{(2\ 0\ 0)}$ = 3.6537 Å. Sanidine was identified using PDF card # 00–025-0618 using the major reflections and d-values of $d_{(2\ 2\ 0)}$ = 3.3300 Å, $d_{(2\ 0\ \bar{2})}$ = 3.2800 Å, $d_{(0\ 0\ 2)}$ = 3.2300 Å, $d_{(\bar{1}\ 1\ 2)}$ = 3.4600 Å, $d_{(\bar{1}\ 3\ 0)}$ = 3.7900 Å, $d_{(\bar{2}\ 0\ 1)}$ = 4.2400 Å, and the lesser reflections and d-values of $d_{(1\ 1\ 0)}$ = 6.6500 Å, $d_{(0\ 2\ 0)}$ = 6.5200 Å, and $d_{(0\ 0\ 1)}$ 6.4500 Å. Calcite was identified using PDF card # 00–047-1743 using the major reflections and d-values of $d_{(1\ 0\ 4)}$ = 3.0355 Å, $d_{(1\ 1\ \bar{3})}$ = 2.2846 Å, and $d_{(1\ 1\ \bar{6})}$ = 1.8753 Å. Magnesian calcite was identified using PDF card # 00-043-0697 using the major reflections and d-values of $d_{(1\ 0\ 4)}$ = 3.0042 Å, $d_{(1\ 1\ 3)}$ = 2.2625 Å, and $d_{(0\ 1\ 8)}$ = 1.8892 Å.

3.6. X-ray fluorescence: bulk elemental compositions

Table 2 reports the bulk major element oxide data for the 10 sampled sands. Also shown are the maximum and minimum abundances for each wt% oxide, the average abundance of each wt% oxide, and their associated standard deviations. Table 3 reports the bulk trace element data for 3 selected sands, one from the start of the sampling transect, one in the middle, and one at the end (TSD 1, TSD 5, and TSD 10). Also reported in Table 3 are the bulk trace element compositions of Earth's crustal geochemical reservoirs (the upper, middle, lower, and bulk continental crust from Rudnick and Gao, 2003).

Fig. 7a summarizes the bulk major oxide abundances of each sampled sand (normalized to 100%). The abundances of these major oxides in Earth's crustal reservoirs are also shown for comparison. Sampled sands are dominated by wt% SiO_2 and wt% Al_2O_3 which combined comprise ~90% of the sand's major element composition, consistent with the abundance of quartz and feldspar observed via light microscopy, SEM, and XRD. Fig. 7b summarizes the relative abundance of the remaining major oxides (normalized to 100%). As shown, wt%. K_2O, Na_2O, and CaO dominate the remaining bulk chemical signature (~80% of total remaining), with wt% Fe_2O_3 and MgO present at the few wt% level (Fig. 7a). Collectively, these signatures are consistent with the abundance of feldspar and the presence of mafic minerals either as individual grains or as basaltic lithics as noted earlier. From Fig. 7b, wt% TiO_2 is the next most abundant major element oxide, consistent with the presence of ilmenite and/or rutile. When compared to Earth's crustal reservoirs, the bulk compositions of the sampled sands are geochemically similar to the upper continental crust, although are slightly more silica rich (by 3–9 wt%). The ferromagnesian component of the sampled sands is also lower than in any of the bulk crustal reservoirs, whereas the alkalic component is higher (wt% Na_2O + K_2O). Fig. 7c summarizes the wt. CaO vs. wt% K_2O characteristics for sampled sands and nearby by dune fields for which comparison data was available (Zimbelman and Williams, 2002; Muhs et al., 2017). With respect to wt% CaO, Tonopah sands are similar to the Cadiz, Danby,

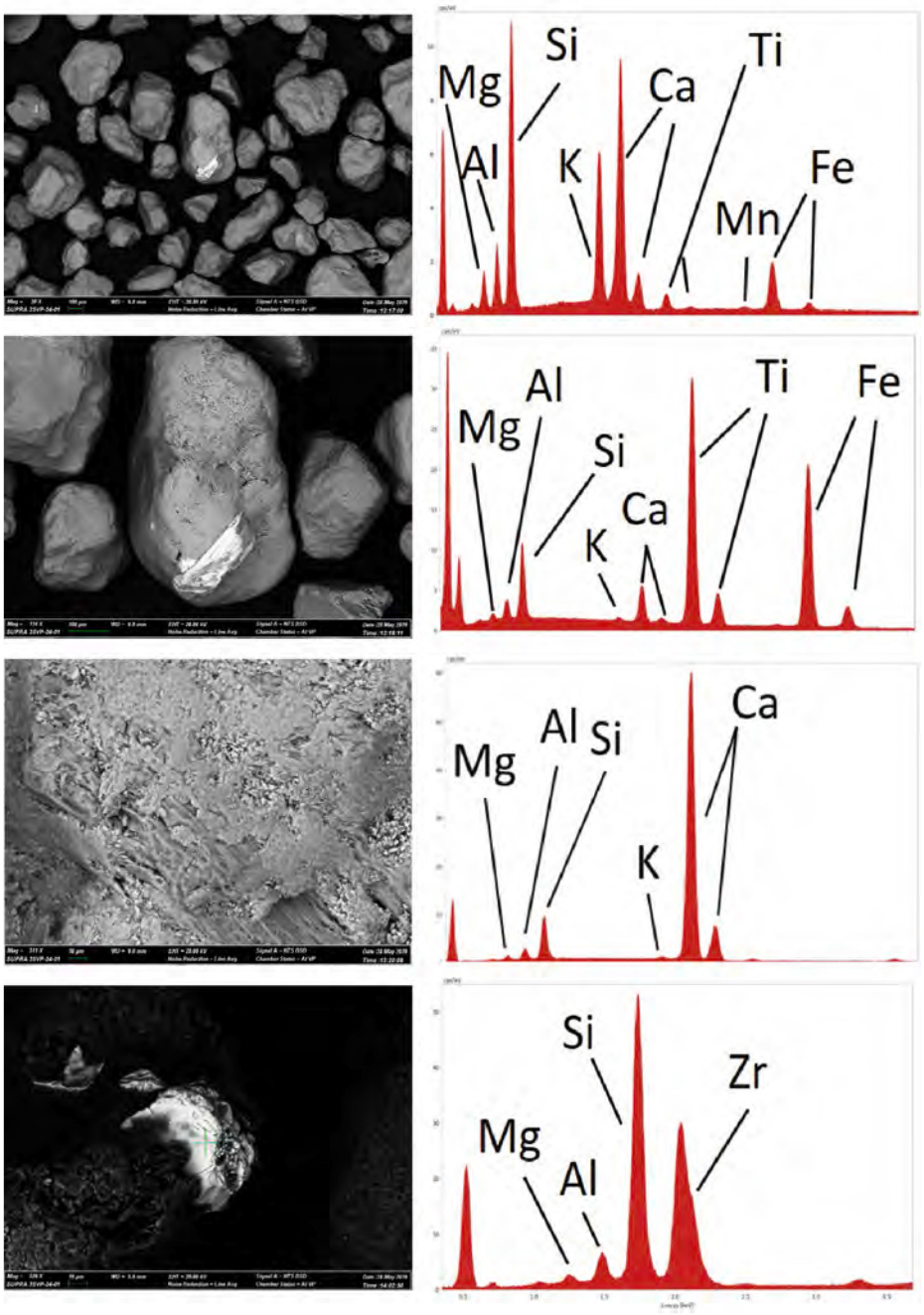

Fig. 5. Representative scanning electron microscope images of subangular to subrounded sand grains. Grains exhibit a range of textures and types. The upper two panels show lithic fragments which are common and often have iron oxides or iron titanium oxides present (bright grains). The K, Si, Al and minor Mg and Fe of the center grain in the top image are consistent with a rhyolite clast. The upper center image and corresponding EDS spectra shows that the Fe-Ti oxide is consistent with ilmenite. The lower central image is interpreted as a rare siliciclastic – carbonate grain dominated by calcium carbonate. A poorly expressed rhombohedral cleavage in the left center of the image suggests the calcium carbonate mineral is calcite. Zircons are also common accessory minerals in lithic fragments as shown in the lower image and corresponding EDS spectra. Rectangular grains observed throughout the SEM images are interpreted as sanidine crystals, and larger moderately rounded grains are commonly quartz. Well-rounded grains are comparatively uncommon.

and Dale lake sands of California to the south (see Fig. 1a) and overlap the higher CaO sands of the Parker dunes in Arizona. The Algodones and East Mesa dunes which are further to the south (also in California, see Fig. 1a) are notably more CaO rich, consistent with their QAP characteristics summarized in Fig. 3b. Sands from the Bristol Trough and Clarks Pass area of California; ~20–30 km northwest and west respectively of the Cadiz and Danby dunes (Zimbelman and Williams 2002) are similarly as enriched in wt% CaO as the California Algodones and East Mesa dunes but exhibit similar wt% K_2O compositions to those of Tonopah. From Fig. 3c the Algodones and East Mesa dunes of California and the Parker dunes of Arizona are compositionally similar and distinct from the other sands shown with respect to wt% K_2O compositions: consistently $<$ 3 wt%. This implies a common origin and a source distinct from other sands across California and Nevada shown in Fig. 3c, despite spatial proximity (Fig. 1a). This source is likely Colorado river sediments as previously suggested in Muhs et al. (1995) and Zimbelman and Williams (2002). The relative proportions of major element oxides in sampled sands and Earth's crustal reservoirs are summarized in Fig. 7d,e. In Fig. 7d, bulk SiO_2/Al_2O_3 vs. bulk K_2O/Na_2O is shown, alongside crustal reservoirs. Again, sampled sands are shown to be the most geochemically similar to Earth's upper continental crust with very similar SiO_2/Al_2O_3 signatures at ~4.5–5 and slightly higher K_2O/Na_2O signatures at 1.2–1.7 (compared to 0.9 for the UCC). In Fig. 7e, bulk Na_2O/CaO vs. bulk Fe_2O_3/MgO is shown, highlighting the higher, but also variable, Fe_2O_3/MgO ratio in sampled sands (2.1–4.8) at a Na_2O/CaO ratio of 1.25–1.75 ((higher than all crustal reservoirs). With respect to the variation in Fe_2O_3/MgO, the sands cluster into two groups, one at Fe_2O_3/MgO values between 2 and 3, and one between 4 and 5. This is interpreted to represent variable contributions from basaltic lithic components and the variable presence of ilmenite.

In supplementary Fig. 3a the general relationship between grain size and bulk wt% SiO_2 is summarized, where sands with larger average

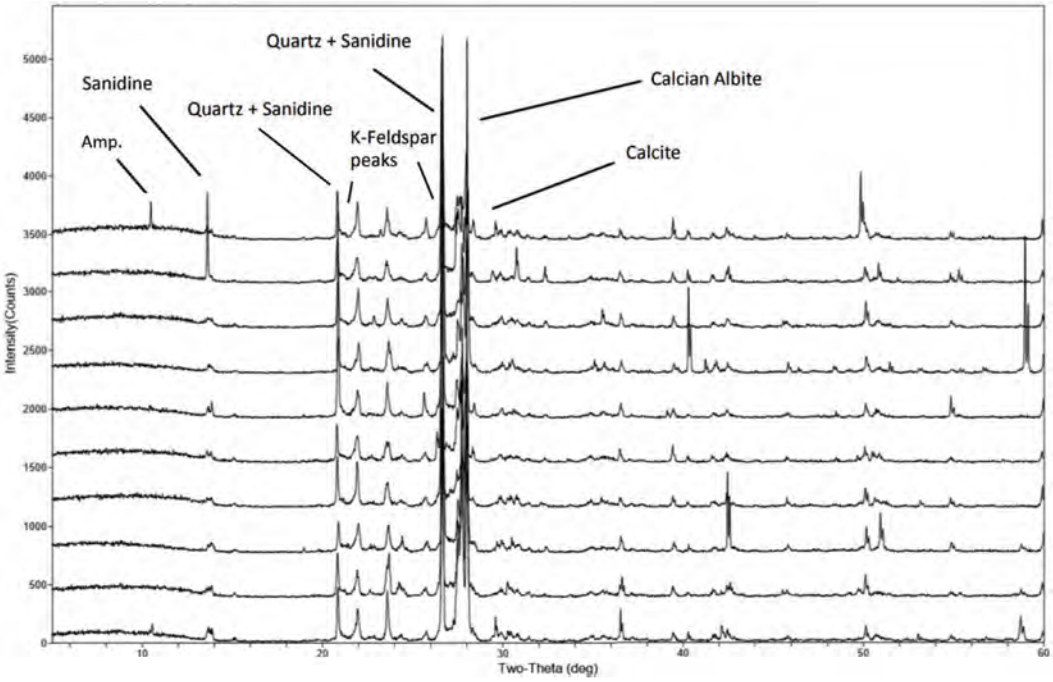

Fig. 6. Minerals identified by X-ray diffraction in sand samples include quartz, ordered calcian albite, sanidine, calcite, and magnesian calcite. Minerals were identified using the computer program Jade and PDF cards.

Table 2
Bulk major element abundances of sampled Tonopah sand dunes. All values reported in wt%

Sample ID	TSD_01	TSD_02	TSD_03	TSD_04	TSD_05	TSD_06	TSD_07	TSD_08	TSD_09	TSD_10	Maximum	Minimum	Average	St. Dev.
P2O5	0.08	0.05	0.07	0.10	0.05	0.10	0.11	0.09	0.13	0.12	0.13	0.05	0.09	0.03
SiO2	70.22	75.41	70.45	68.93	70.94	70.85	69.74	69.91	71.05	68.13	75.41	68.13	70.56	1.94
TiO2	0.05	0.19	0.17	0.27	0.21	0.21	0.22	0.14	0.13	0.26	0.27	0.05	0.18	0.07
Al2O3	15.17	13.41	14.65	14.76	14.47	15.10	15.40	13.90	14.58	15.23	15.40	13.41	14.67	0.62
Fe2O3	1.58	1.03	1.36	1.46	1.52	1.41	1.49	1.28	1.46	1.62	1.62	1.03	1.42	0.17
MgO	0.33	0.24	0.31	0.34	0.56	0.47	0.33	0.61	0.56	0.58	0.61	0.24	0.43	0.14
CaO	2.30	1.72	1.98	2.18	1.82	2.28	2.16	1.96	1.98	2.33	2.33	1.72	2.07	0.21
MnO	0.02	0.02	0.01	0.09	0.04	0.00	0.04	0.03	0.04	0.05	0.09	0.00	0.03	0.02
Na2O	3.40	2.53	3.37	3.56	3.14	2.83	3.23	3.03	2.73	3.43	3.56	2.53	3.12	0.34
K2O	4.45	3.49	4.78	4.35	4.73	4.64	4.48	4.66	4.69	4.12	4.78	3.49	4.44	0.39
LOI	1.47	1.23	1.46	1.52	1.45	1.29	1.33	1.37	1.37	1.22	1.52	1.22	1.37	0.11

grain sizes are higher in bulk wt% SiO_2. This is interpreted as the coarser grained sands containing higher proportions of quartz (and rhyolitic lithic clasts). Supplementary Fig. 3b and 3c highlight the covariance of SiO_2 with K_2O, and Al_2O_3 with Fe_2O_3 respectively. These are interpreted as reflecting the variable presence of quartz and alkali feldspar and the variable presence of mafic components (e.g. basaltic lithics which contain clinopyroxene and plagioclase ± magnetite, ± ilmenite).

In Fig. 8a the bulk trace element, specifically the bulk rare earth element (REE), compositions of the sampled Tonopah sands are summarized. In Fig. 8a, the chondrite-normalized REE abundances of the sands (in red) are shown alongside Earth's crustal geochemical reservoirs (in grey). Consistent with inferences from major element oxide compositions, sampled sands are geochemically similar to the bulk composition of the upper continental crust with similar degrees of light rare earth element enrichment exhibited. The depletion in middle and heavy rare earth elements is however slightly more extreme in the sampled sands when compared to crustal reservoirs with lower Eu-Lu chondrite normalized values. The sands geochemical similarities to the upper crustal reservoir is also demonstrated by their similar $LREE_N/MREE_N$ ratios (as indicated by La_N/Sm_N) at > 4. The REE inter element variation of the sands with respect to the MREEs and HREEs are similar to those of all crustal reservoirs, with Dy_N/Lu_N at 1.2–1.4. From Muhs (2017) the interelement ratios of K/Rb and K/Ba were shown to be reliable identifiers of (geographically) distinct North American dune fields. In Fig. 8b interelement ratios (K/Ba vs. K/Rb) are used to compare and contrast trace element characteristics of regional dune fields to those at Tonopah which exhibit K/Ba from 26 to 31 and K/Rb from 342 to 358. Using these compositional parameters, the Cadiz, Danby, and Dale sands of California are compositionally similar to those of Tonopah and have similar K/Ba ratios to lower range of the Bristol Trough and Clark's Pass (see also, Fig. 7c). The Algodones dunes of California are again distinct with notably higher K/Ba ratios (> 50) and higher K/Rb (> 360), and overlap those of the East Mesa dunes (Muhs, 2017). These similarities have again been used to infer a similar origin, specifically sediments from the shoreline of Lake Cahuilla which are derived from the Colorado River (as discussed in Muhs, 2017).

Of the additional elements analyzed by ICP-MS (Table 3), Pb is the most relevant within the context of human health and broad environmental interest. The concentrations of Pb are 16 ppm in the three samples analyzed. These concentrations are consistent with those from the bulk upper continental crust (17 ppm), as would be expected based on characteristics presented and discussed from Fig. 8a.

Table 3
Bulk trace element abundances of sampled Tonopah sand dunes.

Sample ID							
Ba ppm	1311	1274	1320	628	532	259	456
Th ppm	10.22	10.74	8.74	10.50	6.50	1.20	5.60
Nb ppm	7.02	7.13	6.49	12.00	10.00	5.00	8.00
Y ppm	13.17	13.40	13.08	21.00	20.00	16.00	19.00
Hf ppm	2.75	2.96	2.35	5.30	4.40	1.90	3.70
Ta ppm	0.62	0.62	0.57	0.90	0.60	0.60	0.70
U ppm	2.89	3.03	2.45	2.70	1.30	0.20	1.30
Pb ppm	16.23	16.12	16.10	17.00	15.20	4.00	11.00
Rb ppm	107.9	109.7	95.9	84.0	65.0	11.0	49.0
Cs ppm	4.83	5.04	4.33	4.90	2.20	0.30	2.00
Sr ppm	522	469	572	320	282	348	320
Sc ppm	3.2	3.0	4.4	14.0	19.0	31.0	21.9
Zr ppm	96	107	82	193	149	68	132
La ppm	29.66	30.81	28.60	31.00	24.00	8.00	20.00
Ce ppm	46.62	48.25	46.00	63.00	53.00	20.00	43.00
Pr ppm	6.08	6.23	5.96	6.10	5.80	2.40	4.90
Nd ppm	21.16	21.48	21.22	27.00	25.00	11.00	20.00
Sm ppm	3.80	3.92	3.87	4.70	4.60	2.80	3.90
Eu ppm	0.95	0.92	1.01	1.00	1.40	1.10	1.10
Gd ppm	2.82	2.84	2.86	4.00	4.00	3.10	3.70
Tb ppm	0.43	0.42	0.43	0.70	0.70	0.48	0.60
Dy ppm	2.38	2.46	2.48	3.90	3.80	3.10	3.60
Ho ppm	0.46	0.49	0.47	0.83	0.82	0.68	0.77
Er ppm	1.26	1.29	1.28	2.30	2.30	1.90	2.10
Tm ppm	0.19	0.19	0.19	0.30	0.32	0.24	0.28
Yb ppm	1.19	1.25	1.17	1.96	2.20	1.50	1.90
Lu ppm	0.18	0.20	0.18	0.31	0.40	0.25	0.30

4. Discussion

4.1. Grain size relationships

The grain size distribution and characteristics are expected for an aeolian deposit. From a geochemical perspective, the variation in average grain size (263–335 μm), kurtosis and other grain parameters may explain the variation and lack of correlation of many of the elements (those that did correlate are shown in supplementary Fig. 3). The relative increase of wt% SiO_2 content with grain size is interpreted here as a function of harder, more resistant, quartz grains persisting during transport of the sand with variation explained in part by the occurrence of larger, compositionally variable (basaltic vs. rhyolitic) lithic fragments.

4.2. Mineral identification

It is noted that peaks for major reflections of ordered calcian albite, sanidine and quartz overlap (quartz $d_{(1\ 0\ 1)}$ = 3.3435 Å, quartz $d_{(1\ 0\ 0)}$ = 4.2550 Å; sanidine $d_{(2\ 2\ 0)}$ = 3.3300 Å, sanidine $d_{(\bar{2}\ 0\ 1)}$ = 4.2400 Å; ordered calcian albite $d_{(0\ 0\ 2)}$ = 3.1817 Å, ordered calcian albite $d_{(\bar{2}\ 0\ 2)}$ = 3.1973 Å,) however other peaks confirm the presence of these minerals as does SEM and light microscopy work. The complexity of X-ray diffraction properties of feldspars is well recognized and challenges exist in using powder X-ray diffraction methods for definitively discriminating these minerals on the basis of powder X-ray diffraction alone (e.g., Smith, 1990 and references therein). X-ray diffraction alone is not sufficient to characterize the feldspar mineralogy observed in these samples but the observed variation in the intensities of peaks do show that there are variable amounts of the feldspars present as is supported by the light microscopy data (Fig. 2). Petrographic analysis of sands indicates that there are several minor minerals present that were not detected via powder X-ray diffraction including clinopyroxene and zircon.

4.3. Geochemistry: Sourcing the Tonopah sands

In Fig. 9, the bulk major element oxide compositions of sampled Tonopah sands are used to evaluate their nature and the extent of weathering that is recorded. From Fig. 9a, based on the ratio of Na_2O to K_2O, sampled sands can be classified as quartz-rich with Na_2O/K_2O for all samples $>$ 1. From Fig. 9b, total Al_2O_3 + K_2O + Na_2O vs. wt% SiO_2 is used to evaluate the climate in which the sands were generated with the data implying arid (to potentially semi-arid, one data point) conditions. Fig. 9c summarizes the Chemical Index of Alteration (CIA) for the sampled sands after Nesbit and Young (1982). Values range from 59.93 to 63.44 with an average of 60.34. With respect to CIA values, sampled sands lack clay components (e.g. kaolinite, chlorite, illite) indicating a lack of intensive chemical weathering that would be expected in samples which had experienced significant weathering via chemical processes (where CIA values would likely range from 80 to 100, e.g. Goldberg and Humayun, 2010). This is entirely consistent with the inferences made from Fig. 9b. The CIA values of the Tonopah sands are entirely consistent with values that would be expected in regions were abrasion is dominant over chemical weathering (50–70, Nesbit and Young, 1982).

The quartz-rich nature of the sampled sands alone is initially interpreted here as a consequence of the maturation process. While wind action as a secondary process can lead to the production of quartz-rich sands (e.g., Muhs, 2004), it is also likely that the source rocks to the Tonopah sands were quartz-bearing. The bulk major element chemistry and mineralogy is used here to further evaluate the provenance of the Tonopah sands. From Fig. 9d compositions associated with the parameters DCF 1 and DCF 2 (see caption for details) are consistent with derivation of the sands from a felsic igneous province. This, along with the presence of both basaltic and rhyolitic lithics, is indicative of local sources to the sands due to the extensive outcrops of chemically evolved volcanic sequences in close proximity to Tonopah which were recently comprehensively characterized with respect to their mineralogy and bulk elemental geochemistry in a USGS report (du Bray et al., 2019, see discussion later). The Q-F-L ternary diagram in Fig. 9e (after Dickinson et al., 1983) records a “recycled orogen” for the tectonic setting of the sampled sands. Within the context of the fields shown in Fig. 9e, this is interpreted as indicating reworking of igneous (+/- metamorphic) lithologies although it is also noted here that no metamorphic lithics were observed during polarized microscopy or SEM study (Fig. 2).

In Fig. 10, the major and trace geochemical characteristics of the Tonopah sands are collectively used to highlight and summarize the similarities and differences between sampled sands and Earth’s crustal geochemical reservoirs. Relative enrichments and depletions are highlighted. When all geochemical signatures are considered, the sampled sands are most geochemically similar to that of the upper continental crust with ratios of SiO_2, Al_2O_3, Na_2O, La, Pr, Eu, Th, U, Pb, Cs in the sand to UCC at ~1. Only 3 chemical components in the sand are enriched over the UCC at $>$ 1.5: K_2O, Ba, and Sr, with Rb being the only other element that also shows relative enrichment (at $>$ 1, $<$ 1.5). Interestingly, all of these chemical components are associated with alkali and/or plagioclase feldspar with K_2O being an essential component of alkali feldspar and Rb^+, Ba^{2+} and Sr^{2+} substituting into the K^+ or Ca^{2+} sites in alkali and plagioclase respectively. Collectively, these relative enrichments are interpreted as reflecting the relatively high contribution from chemically evolved, felsic source materials to the Tonopah sand dunes. Five of the chemical components reported for the sampled sands consistently show depletion ($<$ 0.5) relative to the UCC reservoir: TiO_2, Fe_2O_3, MgO, MnO, and Sc. Interestingly, all of these chemical components are common in minerals which would otherwise be found in mafic lithologies with Fe_2O_3 and MgO important constituents of olivine, the pyroxenes, and magnetite (Fe_2O_3), and TiO_2 (with Fe_2O_3) constituting ilmenite. Both Mn and Sc are compatible in clinopyroxene and ilmenite, with Mn also partitioning into magnetite. Collectively, these relative depletions are interpreted as reflecting the relatively low contribution from mafic materials to the Tonopah sand dunes.

In order to further provide global and broad scale regional context

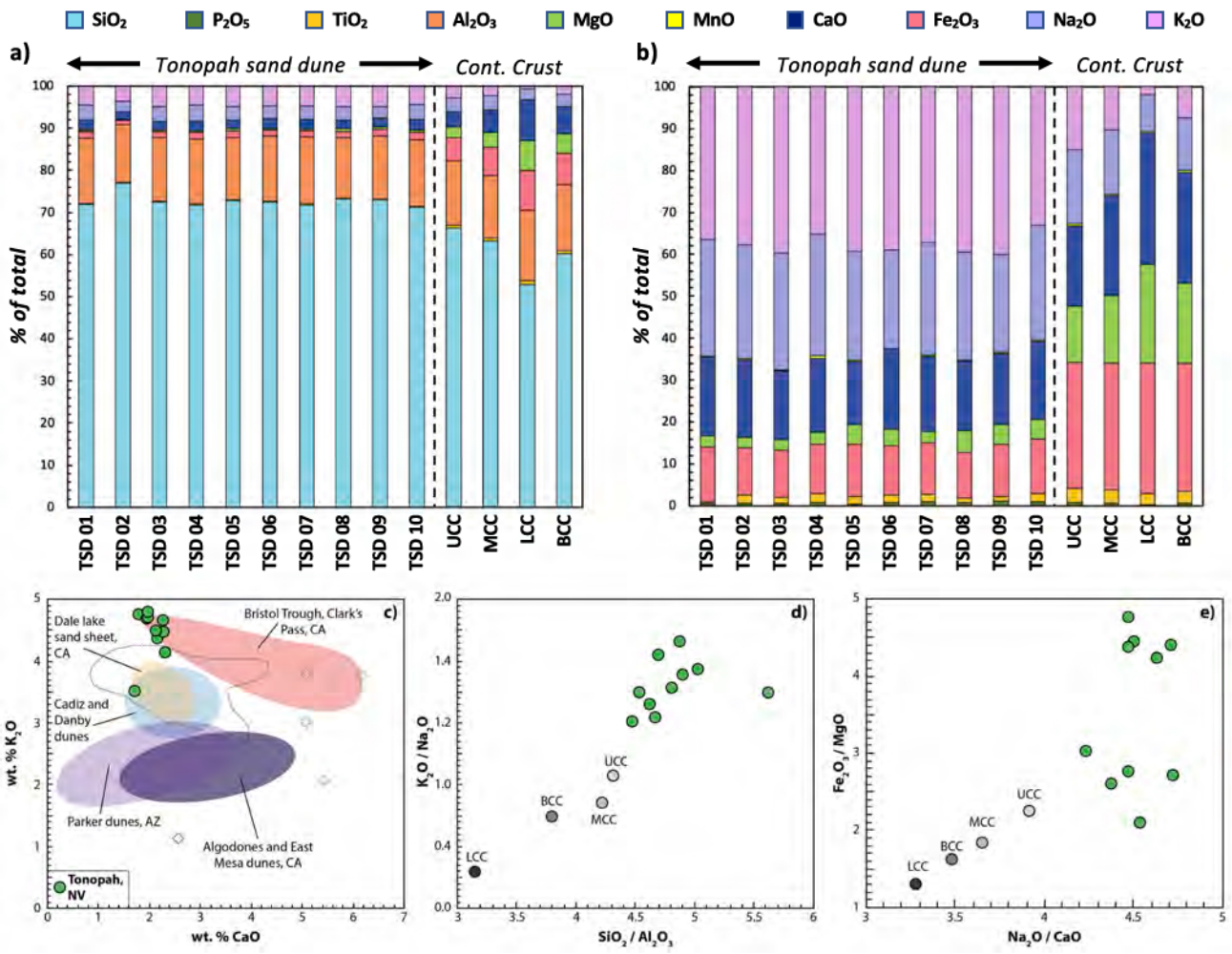

Fig. 7. (a) Bulk major element oxide compositions of sampled Tonopah Sand Dunes compared to bulk major element oxide data for Earth's crustal geochemical reservoirs. UCC: Upper Continental Crust; MCC: Middle Continental Crust; LCC: Lower Continental Crust; BCC: Bulk Continental Crust. Data from Rudnick and Gao (2003). As shown, SiO_2 and Al_2O_3 dominate the bulk major element chemistry of sampled sand (tightly constrained at 88–92 wt% of total between all 10 samples), consistent with the abundance of quartz and feldspar. Compared to bulk crustal reservoirs, the sand dunes are compositionally the most similar to the UCC reservoir. (b) Bulk major element oxides (as wt%), excluding SiO_2 and Al_2O_3. With respect to the major elements which contribute 8–12 wt% of the sampled sand dunes, K_2O, Na_2O, and CaO dominate. This is entirely consistent with the abundance of feldspar minerals observed. By comparison to bulk crustal reservoirs, the proportions of these particular major oxides are higher although inter- major element oxide ratios are similar to that of the UCC reservoir. (c) wt% CaO vs. wt% K_2O comparing sampled Tonopah sands to select nearby dune fields across the western US (for dune field location see Fig. 1). Data from: Zimbelman and Williams (2002), Muhs et al. (2017). (d) SiO_2/Al_2O_3 vs. K_2O/Na_2O signatures for sampled sand dune compared to bulk crustal geochemical reservoirs. With respect to both of these parameters, samples are again most similar to the UCC reservoir, particularly SiO_2/Al_2O_3. e) Na_2O/CaO vs. Fe_2O_3/MgO signatures for sampled sand dune compared to bulk crustal geochemical reservoirs. With respect to both of these parameters, samples are again most similar to the UCC reservoir, particularly Fe_2O_3/MgO. (f) Bulk wt% Na_2O vs. wt% K_2O applied to assess extent of quartz dominance. Consistently, sampled sands plot as Quartz-rich at $Na_2O/K_2O > 1$. (g) Bulk wt% $Al_2O_3 + K_2O + Na_2O$ vs. wt% SiO_2 applied as an evaluation of humidity or aridity. Consistently, sampled sands plot as being derived from an arid environment. h) Assessment of sand dune provenance: DCF 1: $(-1.773*TiO_2) + (0.607*Al_2O_3) + (0.76*Fe_2O_3) + (-1.5*MgO) + (0.616*CaO) + (0.509*Na_2O) + (-1.224*K_2O) + (-9.09)$ vs. DCF 2: $(0.445*TiO_2) + (0.07*Al_2O_3) + (-0.25*Fe_2O_3)$. Consistently, sampled sands plot as being derived from a felsic igneous province.

for the studied Tonopah sands, major element oxides are compared to dune fields from across the world in Fig. 11a and the central-western US in Fig. 11b. In both cases Log (SiO_2/Al_2O_3) vs. Log (Na_2O/K_2O) values are shown as proxies for mineralogical maturity (after Pettijohn et al., 1973, modified from Muhs, 2017). Here, sands which are more mature will have higher Log (SiO_2/Al_2O_3) at lower Log (Na_2O/K_2O) due to the increased presence of quartz and increasing lack of feldspar, while Log (Na_2O/K_2O) specifically accounts for the contribution from plagioclase vs. alkali feldspar (i.e. depletion in plagioclase due to more resistant alkali feldspar, Muhs, 2017). Compared to active and Holocene-aged dunes in the US, global dune systems exhibit the same range of variability. Considering these compositional parameters, the Tonopah sands are comparable to those of the Taklamakan Desert in southwest Xinjiang, western China and are classified here as greywackes (and perhaps as weak lithic arenites). Within global contexts the Tonopah sands are distinctly quartz-poor (Log $(SiO_2/Al_2O_3) < 1$) and relatively immature. Compared to dune fields in the US Tonopah sands are the most similar to those of the Mojave Desert, California with very similar ranges of Log (SiO_2/Al_2O_3) values: 0.65–0.80. These values are notably lower than other dune fields across the US which are demonstrably more mature (up to quartz arenite) with corresponding Log (SiO_2/Al_2O_3) values up to ~2.3 (the Monahans dunes of west Texas). Consistent with previous observations the Tonopah sands specifically exhibit similar chemical characteristics to the Cadiz, Danby, and Dale lake sands (see map in Figs. 1a, 7c, 8b). These are represented in Fig. 11b by the Mojave Desert compositional field. Again, consistent with previous observations sampled Tonopah sands are compositionally distinct from the Algodones dunes to the south in California and the Parker dunes of

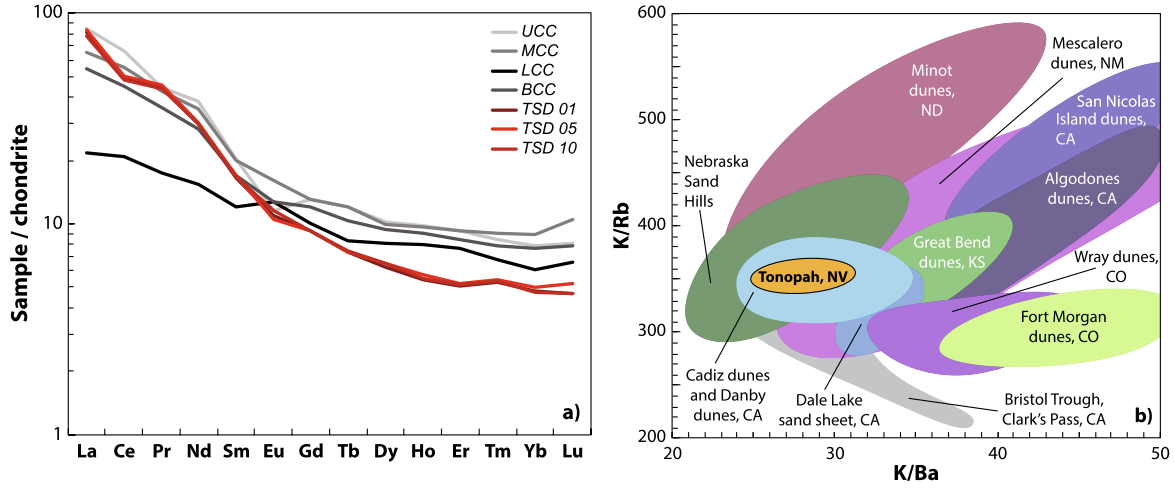

Fig. 8. (a) Chondrite-normalized REE plot of sampled sands compared to the bulk REE geochemistry of Earth's crustal reservoirs. Sands show LREE enrichment over the MREEs, and MREE enrichment over the HREEs. (b) K/Ba vs. K/Rb for sampled Tonopah sands compared to regional dune fields. Figure modified from Muhs (2017). Data from Pepe (2014) for Bristol Trough (Cadiz and Danby dune fields) and Clark's Pass, CA, also included.

Arizona (see map in Figs. 1a, 7c, 8b). Both of these dune fields are mineralogically more mature (Log (SiO_2/Al_2O_3) 1–1.5) and are classified as sub-arkose to sublithic-arenite in Fig. 11b. Regionally this is consistent with the Mojave Desert sand dune fields and the Tonopah sands being derived from a source (or sources) distinct from that of the Algodones (and Parker) dunes despite their close spatial proximity (Zimbelman and Williams, 2002; Muhs et al., 2003; Muhs, 2017). This can be accounted for (as discussed in Muhs et al. 2003) by the Colorado River acting as a barrier to sediment transport from the Mojave Desert region eastward. While the mineralogically mature Algodones and Parker dunes are ultimately associated with derivation from Colorado River sediments, the mineralogically less mature Mojave Desert sands (Danby, Cadiz, and Dale lake) have origins associated with chemically evolved granodiorite/granite-derived alluvium, likely derived from surrounding mountain ranges (e.g. the Coxcomb, Old Woman, and Turtle Mountains; see Fig. 10 in Muhs, 2017). Due to the similarity between the Tonopah sands and these Mojave Desert sand dune fields, Tonopah sands are therefore interpreted to also be derived from chemically evolved igneous sources. This is explored and discussed on a more regional and local scale below.

In order to further evaluate regional and/or local source(s) to the Tonopah sand dunes, their bulk major element chemistries were compared to the bulk chemical signatures from the surrounding bedrock. Bulk elemental data for these potential sources was accessed through the USGS National Geochemical Database. For the state of Nevada, Nye county (in which Tonopah lies) is the second most well-characterized with respect to sample coverage out of the 17 subdivisions across the state with 6089 samples analyzed (as of Dec. 2019). Comparison between the 10 sampled sands, Earth's bulk crustal reservoirs, and the average Nye County bedrock are shown in Fig. 12 (a-j for each major element oxide). The average composition of the Nye County bedrock is summarized in Table 4. The difference in wt% of the major element oxides between the Nye County bedrock and the sampled sands is summarized in Fig. 12k with each sand plotted for each of the oxides. With respect to bulk chemistry, several of the major element oxides exhibit differences of $<$ 0.5 wt% (P_2O_5, TiO_2, and MnO). These major oxides are typically however associated with the trace and minor phases in crystalline bedrock and so this is not unexpected due to primary abundances in crystalline bedrock being low (see Fig. 13 later). The abundance of wt% Fe_2O_3, MgO, and CaO are also consistently less than the average Nye County bedrock but no more than by 2.5 wt% with Fe_2O_3 from 0.7 to 1.3 wt% less and MgO and CaO at 1.5–2.5 wt%. This interpreted here to again be consistent with the lack of mafic minerals in the sampled sands (see earlier). The remaining major oxides are all enriched relative to Nye County bedrock. Both wt% Na_2O and K_2O are variably enriched up to ~1.5 wt% with K_2O slightly more enriched compared to Na_2O. wt% Al_2O_3 is enriched by 1–3 wt% with wt % SiO_2 enriched by ~2–5 wt% with the exception of one of the samples which is enriched up almost 10 wt%. The collective enrichment in SiO_2 is consistent with the observation and classification of these sands being quartz-rich (Figs. 2, 3, 9a) and the interpretation that not only were the source rocks likely quartz rich but that secondary processing through wind action has worked to mature the sediment.

Of the 21 regions at the 1:250,000 scale classified by the USGS, Tonopah is the second most well-characterized region with 5397 samples analyzed. Fig. 12l and Table 4 summarizes the comparison of the Tonopah sands to the average Tonopah bedrock. Inferences from this are the same as those from the Nye County comparison with similar orders of magnitude with respect to differences observed for each wt.% oxide and the same relative enrichments and depletions observed. The only minor observable differences are that differences in Fe_2O_3 are slightly less at 0.2–0.8 wt% and slightly more for MgO and CaO at 2.4–2.8 and 1.9–2.5 respectively.

In 2019 the USGS released a Scientific Investigations Report on the Petrology and Geochemistry of the volcanic sequences associated with Tonopah and the surrounding mining areas at Divide (6.5 miles south of Tonopah) and Goldfield (28 miles south of Tonopah). Within that report (du Bray et al., 2019), 26 bulk chemical analyses were reported which included analyses of local andesites, trachyandesites, trachytes, dacites, rhyodacites, and rhyolites. The average composition of these potential source rocks was used to compare to the bulk major element chemistry of the Tonopah sand dunes. Results are summarized in Table 4 and in Fig. 13. Differences in wt% P_2O_5, TiO_2, and MnO are similar to both the Nye County and Tonopah datasets (close to 0 at $<$ 0.5 wt%). Differences in wt% Na_2O are typically $<$ 1 wt% with differences in wt% CaO $<$ 2. Notably, differences in wt% Fe_2O_3 are higher by ~2 wt%. With respect to the remaining major element oxides (wt% SiO_2, Al_2O_3, MgO, and K_2O) differences between sampled sands and the average volcanic rocks around Tonopah are less than when compared to the average bedrock compositions considered in Fig. 12k-l (see also, Table 4). Most notable is the comparatively low difference in wt% SiO_2 with values as low as 0.92 wt% for one sample although between 1 and 4 wt% difference is more characteristic.

While the recent data set presented by du Bray et al. (2019) presents an enticing possibility for identifying the source rocks to the Tonopah sand dunes, it is highly likely that they are not the only source although they

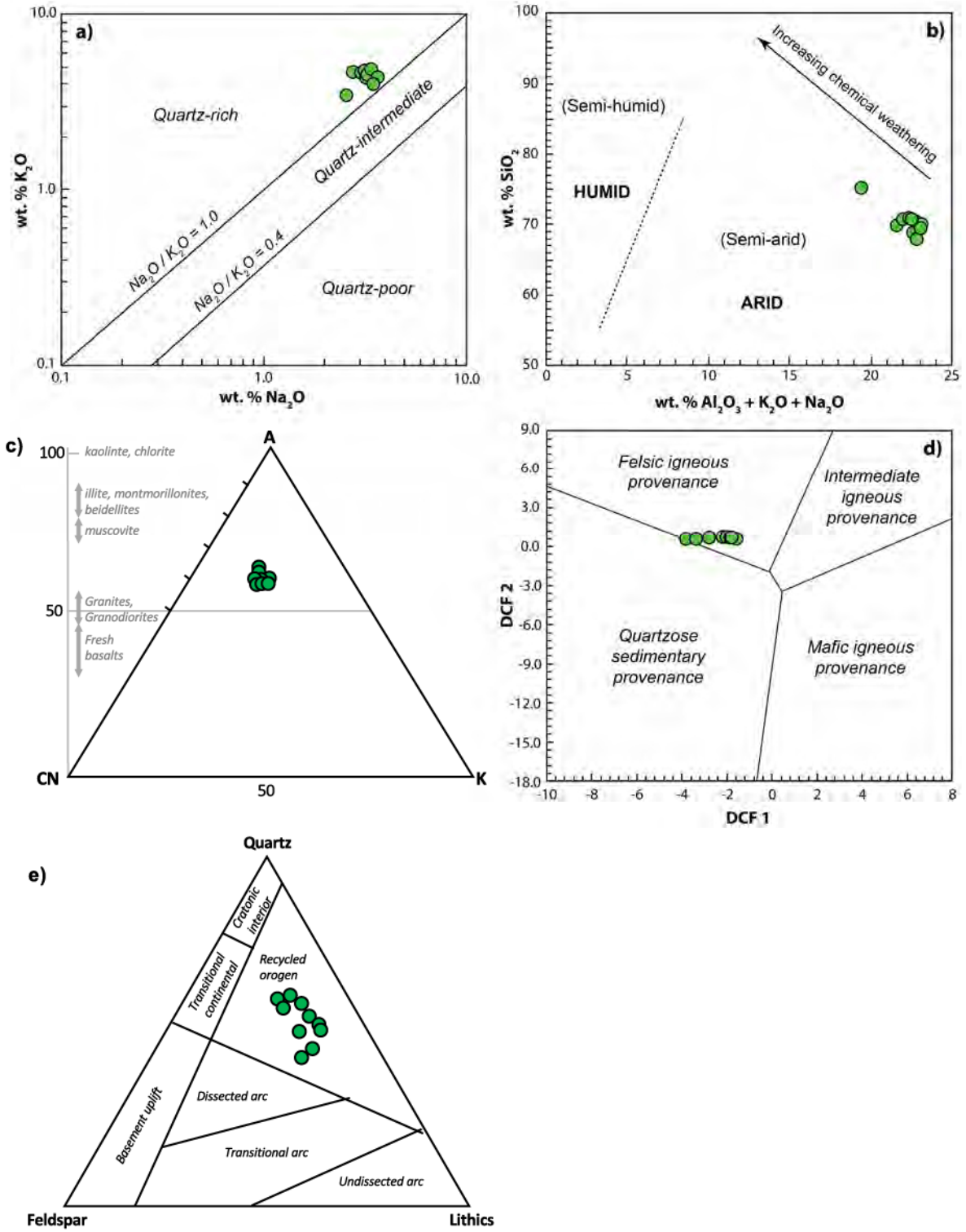

Fig. 9. (a) Chemical Index of Alteration (CIA) after Nesbitt and Young (1982). Tonopah sands exhibit a limited range of values from ~60 to 63. For discussion see text. (b) Quartz-Feldspar-Lithics diagram used to evaluate the tectonic setting of the sampled sands (as would otherwise be inferred by Q-F-L characteristics).

may prove to be the dominant source. This inference is made based on the fact that the dune system studied here is a star dune and that the prevailing wind direction throughout the year does change, although the dominant direction is from north to south (see supplementary Fig. 1). The relative lack of mafic lithics supports derivation from chemically evolved sources yet they are present (Fig. 2) hence the Tertiary basalts which outcrop a few miles to north and east of Tonopah are likely to also be contributing. These inferences regarding sand provenance can however be easily tested by future studies. For example, the volcanic rocks in du Bray et al. (2019) were reported to have been erupted and emplaced over a time frame of 21 Ma to 12 Ma (depending on the individual unit) as constrained by Ar-Ar in allanite, plagioclase, and sanidine as well as U-Pb in zircon. While allanite was not identified in sampled sands, abundant feldspars and zircon was hence these grains could be targeted for future geochronological analysis in order to further investigate the source material(s) to the Tonopah Crescent dunes.

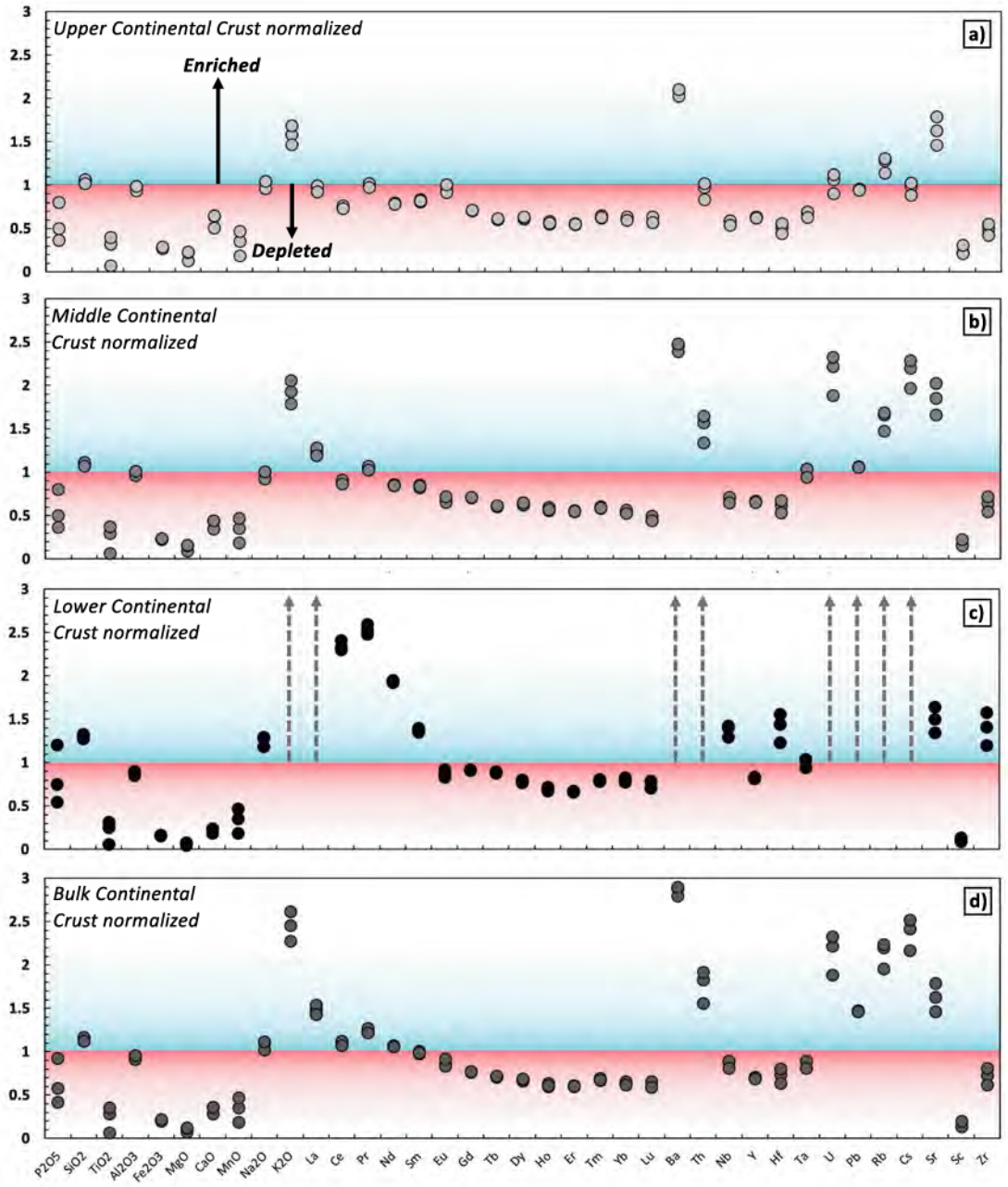

Fig. 10. Summary of relative enrichment and depletion of major oxide and trace elemental compositions from the three sampled sands for which both major and trace element data was collected, normalized to values from Earth's crustal reservoirs. All shown at the same scale (y-axis). Where values exceed this, dotted arrows are shown (only LCC-normalized). For discussion, see text.

4.4. Providing environmental context

Sands from the large southern dune north of Tonopah should be considered as an appropriate environmental reference material for central Tonopah because the dune is located 15 km to the north-northwest west of the town, yet the dune is a star dune (Fig. 1c,d), and therefore receives sediment contributions from all directions. However, there are several factors that need to be considered if these dune sands are to be utilized as an environmental reference in the strict sense. Tonopah has mild seasonal variation of wind, measured at a 10 m height, over the year with more wind between mid-February to mid-June with an average of 8.1 miles per hour, and less wind in the remaining months with an average of 6.9 miles per hour. Wind direction is variable throughout the year. Wind is primarily from the south for approximately 3.5 months for an average time frame of from June 17 to September 29, The wind is most often from the north for the remaining 8.5 months, from September 29 to June 17 (weatherspark.com, see also, supplementary Fig. 1). Accordingly, the wind direction from the south would work to permit transport of silver mine waste material that remains exposed in the town of Tonopah today to be deposited in the dune (although no evidence of this was found by this study).

Compared to other regions of the country, Nevada has had comparatively few investigations in the area of metal pollution whether that pollution originated from mine waste or other sources. There have been a series of investigations centered on Hg (Eckley et al., 2011; Heyvaert et al., 2000; Cizdziel et al., 2003; Henny et al., 2002; Miller et al., 1998; Miller et al., 1996) but investigations of multiple metals within the

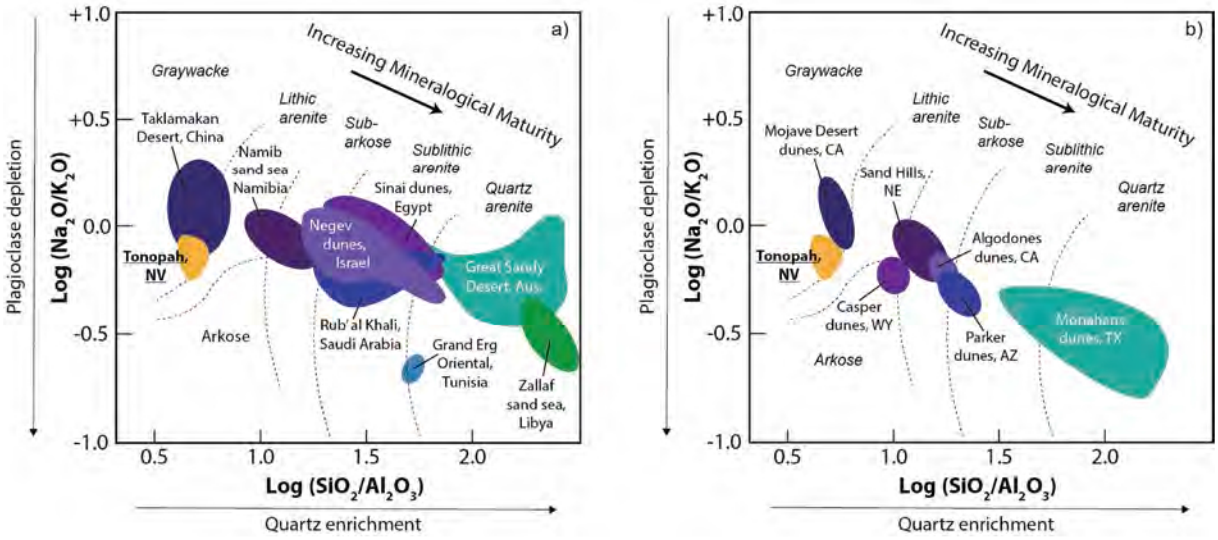

Fig. 11. a) and b) show Log (SiO_2/Al_2O_3) vs. Log (Na_2O/K_2O) values as proxies for the mineralogical maturity (after Pettijohn et al., 1973) of sampled Tonopah sands in addition to global datasets (a) and dune fields across the central and western US (b). Modified from Muhs (2017). Tonopah sands are regionally the most similar to the sand dunes of the Mojave Desert, CA. For discussion see text.

same study is comparatively less common (Sims et al., 2013; Sims, 2010; and Yang et al., 2003). For example, specialized investigations of W pollution have been conducted in Fallon, NV, (Sheppard et al., 2012, 2007) while Kersting et al., (1999) investigated Pu. Soukup et al. (2012) observed As in the Nellis Dunes recreational area near Las Vegas reporting concentrations between 0.42 and 14.71 ppm while a later study (Goossens et al., 2015) found concentrations of As up to 7058 ppm in topsoil and bedrock.

One metal that is noted here as not having been extensively investigated in broad environmental studies in these environments in Nevada is Pb. Lead is well established as a toxin that affects a wide variety of bodily systems including neurological, renal, cardiovascular, hematological, immunological, reproductive, and developmental effects (e.g., Gostin 2016; Grandjean and Landrigan 2014; Grandjean 2010; Ko et al 2007; Lanphear et al 2005; Needleman 2004; Jarup 2003). For example, ATSDR (2019) data indicates that Pb is a particularly harmful pollutant and that children are more susceptible to the health effects of Pb owing to due to the greater gastrointestinal absorption of ingested Pb, more frequent hand-to-mouth activities, and a more vulnerable central nervous systems (e.g., Huang et al. 2016; Ko et al. 2007; Needleman 2004; Stewart et al. 2014). Lead can negatively impact children's mood and behaviors, cognitive function, contribute to learning deficiencies and alter neuromotor and neurosensory functions. In adults, it decreases cognitive function such as memory, attention, learning capacity, and alters mood and behaviors. Furthermore, the agency shows that lead has been shown to increase the risk of heart disease leading to increased mortality, decrease an individual's resistance to disease, trends in autoimmunity and anemia, and decreases fertility in both males and females. There are now clear indications that even minimal exposure to Pb has proven to have significant negative effects which supports the position that there are no safe levels of environmental Pb exposure (Gostin 2016; Grandjean 2010; Grandjean and Landrigan 2014; Lanphear et al. 2005).

Lead pollution in central and western Nevada is likely owing to the extensive mining history, military activity, and transportation corridors and towns such a Tonopah are likely to be impacted. Yet this remains unconstrained at present. The Pb concentrations observed in this study (at ~16 ppm and consistent with those expected for Earth's bulk upper continental crust, see Table 3), combined with the comprehensive mineralogical and geochemical analyses indicate that these sands would be an appropriate environmental reference for future pollution studies for Tonopah and other regions across central and western Nevada. Similar detailed studies involving reference materials such as LeGalley et al. (2013) and Barnes et al. (2020) help provide constraints on local and regional pollution with ample context.

This investigation also has direct impact on local communities by supporting funded studies and community organizations with geogenic background information that would not otherwise be provided. In particular, results from this study will support ongoing environmental efforts in Nye County by serving as important environmental reference materials. In 2018 Nye County was awarded a total of $800,000 in federal grants from the U.S. Environmental Protection Agency for Brownfields environmental cleanup efforts on distressed tribal properties, mine-scarred lands, abandoned automotive stations and aged buildings with hazardous structural materials (Nye County, 2018). This funding will capitalize a revolving loan fund where Nye County will provide up to four loans and one subgrant to support cleanup efforts for contaminated sites with $200,00 allocated for petroleum sites and $600,000 allocated for hazardous substances. Results of our investigation will be particularly useful for providing information on not only geogenic backgrounds but also the nature of sediment for organizations such as the Rural Desert Southwest Brownfields Coalition (RDSBC). This organization works to improve economically disadvantaged communities and provides funding and assistance to transform contaminated sites into assets that can spur economic growth. The RDSBC's region is characterized by underserved and rural communities that have inherited brownfield problems. Data provided by this study has the potential to impact environmental decision making in addition to adding regional geochemical context, thus providing both economic and environmental value.

4.5. Implications for future hyperspectral remote sensing and climate studies

The reflective spectra collected on the Tonopah sands are consistent with the observed mineralogy and geochemistry with most features being associated with water or OH groups. The reflective spectra of the sands show minimal variation although there is modest variation of the mineralogy and bulk geochemical composition (as has been presented and discussed). Reflective spectra should be of significant utility for future environmental studies. Hyperspectral remote sensing (HRS) continues to grow significantly as a tool to investigate the environment throughout applications throughout the Earth Sciences (e.g., geology: Sabins, 1999; Hörig et al., 2001; Kruse et al., 2003; Crouvi et al. 2006; Bishop et al., 2011; Cracknell and Reading, 2014; climate change: e.g.,

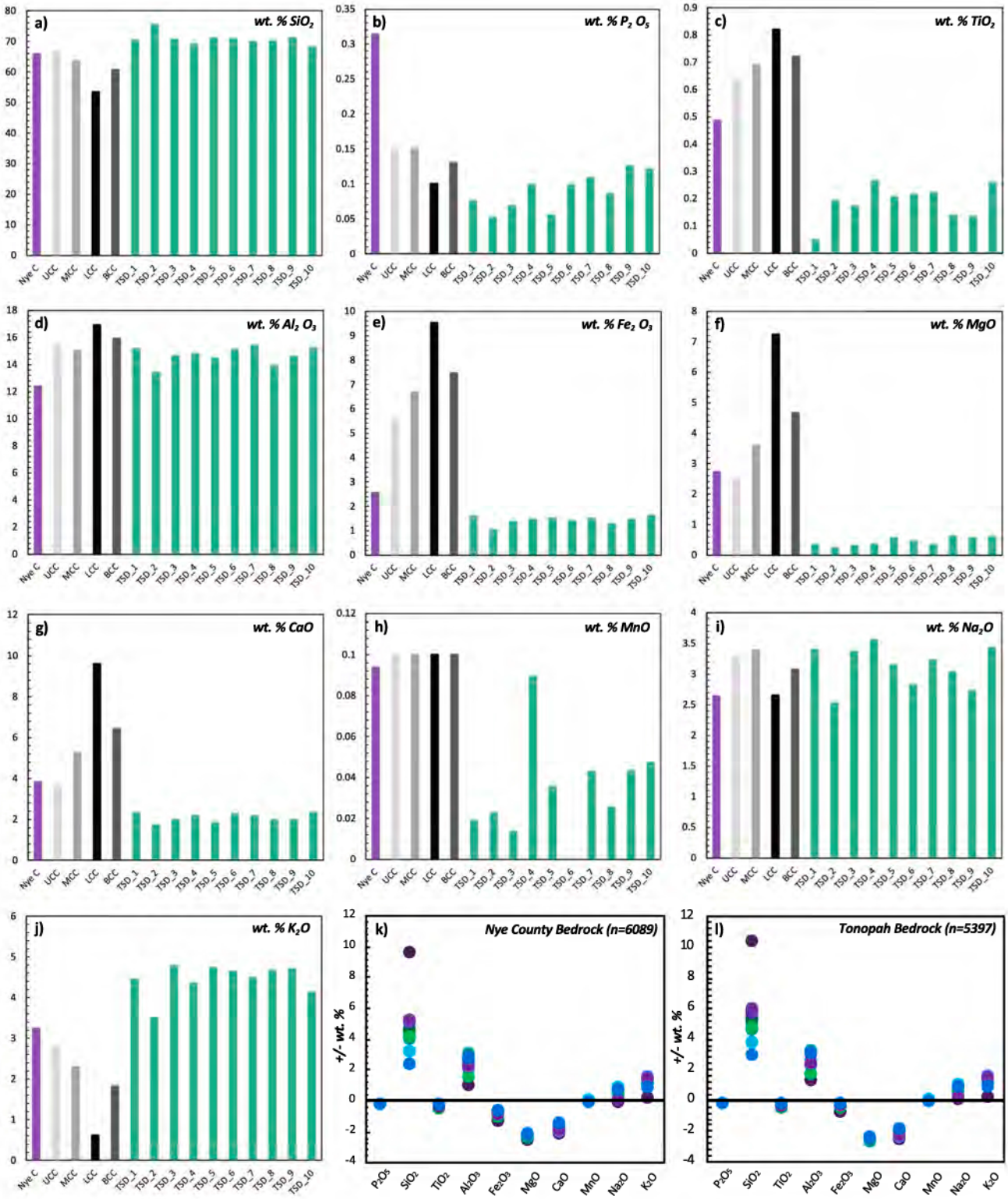

Fig. 12. Comparison of bulk elemental characteristics of Tonopah sand to Earth's bulk crustal reservoirs (as presented earlier) and the average bedrock composition of Nye County (panels a-k). Data for Nye County accessed from the United States Geological Survey (USGS) National Geochemical Database (n = 6089 samples for Nye County). In panel k, relative enrichment and depletions, presented as +/- wt% of that oxide, are presented with all reported major oxides of the Tonopah sand within +/-2 wt% of the average Nye County bedrock (as characterized by USGS data). In panel l), the same data is summarized but presented here in comparison to data available for Tonopah (available from the USGS National Geochemical Database (n = 5397 samples for Tonopah).

Aumann et al. 2005; Ustin et al., 2009; environmental contamination e.g., Swayze et al., 2000; Mars and Crowley, 2003; Choe et al., 2008; Krekeler and Allen, 2008; Allen and Krekeler, 2011; Leifer et al., 2012; and wildlife e.g., Ustin et al., 2002; Carlson et al., 2007; Leblanc et al., 2016). There are previous studies reporting results from hyperspectral imaging of various settings in Nevada and adjacent regions (e.g., Davies

Table 4
Bulk major element comparisons between sampled Tonopah sands and potential sources.

Tonopah (USGS Geochemical Database)										
	P2O5	SiO2	TiO2	Al2O3	Fe2O3	MgO	CaO	MnO	Na2O	K2O
	0.35	***65.14***	***0.52***	***12.2***	***1.82***	***2.98***	***4.25***	***0.09***	***2.5***	***3.25***
TSD_1	−0.27	5.08	−0.47	2.97	−0.24	−2.65	−1.95	−0.07	0.90	1.20
TSD_2	−0.30	10.27	−0.33	1.21	−0.79	−2.74	−2.53	−0.07	0.03	0.24
TSD_3	−0.28	5.31	−0.35	2.45	−0.46	−2.67	−2.27	−0.08	0.87	1.53
TSD_4	−0.25	3.79	−0.25	2.56	−0.36	−2.64	−2.07	0.00	1.06	1.10
TSD_5	−0.30	5.80	−0.31	2.27	−0.30	−2.42	−2.43	−0.05	0.64	1.48
TSD_6	−0.25	5.71	−0.31	2.90	−0.41	−2.51	−1.97	−0.09	0.33	1.39
TSD_7	−0.24	4.60	−0.30	3.20	−0.33	−2.65	−2.09	−0.05	0.73	1.23
TSD_8	−0.26	4.77	−0.38	1.70	−0.54	−2.37	−2.29	−0.06	0.53	1.41
TSD_9	−0.22	5.91	−0.39	2.38	−0.36	−2.42	−2.27	−0.05	0.23	1.44
TSD_10	−0.23	2.99	−0.26	3.03	−0.20	−2.40	−1.92	−0.04	0.93	0.87
Nye County (USGS Geochemical Database)										
	P2O5	SiO2	TiO2	Al2O3	Fe2O3	MgO	CaO	MnO	Na2O	K2O
	0.31	***65.78***	***0.49***	***12.39***	***2.31***	***2.73***	***3.82***	***0.09***	***2.64***	***3.22***
TSD_1	−0.23	4.45	−0.44	2.78	−0.73	−2.40	−1.52	−0.07	0.76	1.22
TSD_2	−0.26	9.64	−0.29	1.02	−1.28	−2.49	−2.10	−0.07	−0.11	0.26
TSD_3	−0.24	4.68	−0.31	2.26	−0.95	−2.42	−1.84	−0.08	0.73	1.55
TSD_4	−0.21	3.16	−0.22	2.37	−0.85	−2.39	−1.64	0.00	0.92	1.12
TSD_5	−0.26	5.17	−0.28	2.08	−0.79	−2.17	−2.00	−0.06	0.50	1.50
TSD_6	−0.21	5.08	−0.27	2.71	−0.90	−2.26	−1.53	−0.09	0.19	1.42
TSD_7	−0.20	3.97	−0.26	3.01	−0.82	−2.40	−1.66	−0.05	0.59	1.25
TSD_8	−0.22	4.14	−0.35	1.51	−1.03	−2.12	−1.86	−0.07	0.39	1.43
TSD_9	−0.18	5.28	−0.35	2.19	−0.85	−2.17	−1.84	−0.05	0.09	1.46
TSD_10	−0.19	2.36	−0.23	2.84	−0.69	−2.14	−1.49	−0.05	0.79	0.90
du Bray et al. (2019)										
	P2O5	SiO2	TiO2	Al2O3	Fe2O3	MgO	CaO	MnO	Na2O	K2O
	0.25	***67.21***	***0.57***	***15.59***	***3.61***	***1.5***	***3.6***	***0.07***	***3.62***	***3.97***
TSD_1	−0.17	3.01	−0.52	−0.42	−2.03	−1.17	−1.30	−0.05	−0.22	0.48
TSD_2	−0.20	8.20	−0.38	−2.18	−2.58	−1.26	−1.88	−0.05	−1.09	−0.48
TSD_3	−0.18	3.24	−0.40	−0.94	−2.25	−1.19	−1.62	−0.06	−0.25	0.81
TSD_4	−0.15	1.72	−0.30	−0.83	−2.15	−1.16	−1.42	0.02	−0.06	0.38
TSD_5	−0.20	3.73	−0.36	−1.12	−2.09	−0.94	−1.78	−0.03	−0.48	0.76
TSD_6	−0.15	3.64	−0.36	−0.49	−2.20	−1.03	−1.32	−0.07	−0.79	0.67
TSD_7	−0.14	2.53	−0.35	−0.19	−2.12	−1.17	−1.44	−0.03	−0.39	0.51
TSD_8	−0.16	2.70	−0.43	−1.69	−2.33	−0.89	−1.64	−0.04	−0.59	0.69
TSD_9	−0.12	3.84	−0.44	−1.01	−2.15	−0.94	−1.62	−0.03	−0.89	0.72
TSD_10	−0.13	0.92	−0.31	−0.36	−1.99	−0.92	−1.27	−0.02	−0.19	0.15

and Calvin, 2017; Mars and Crowley 2003). Having well-characterized substrates such as the Tonopah sands is therefore important for reference materials within these contexts and can serve numerous purposes across multiple disciplines working in Nevada. The Tonopah sands can be therefore used in both field experiments in the region and direct observation and investigation of hyperspectral imagery in the context of ecology, mine waste studies, and even nearby military research and development operations.

By comprehensively documenting the mineralogical and geochemical characteristics of the Tonopah sand dunes this study therefore presents much needed context for future work across the region.

5. Conclusions

The comprehensive mineralogical and geochemical characterization of the Tonopah sands studied here has established the regional geogenic background and therefore serves as an important environmental reference material for future studies of dune systems and metal pollution across the region. Sampled sands are quartz-rich as observed via polarized light microscopy, scanning electron microscopy, reflective spectroscopy and as defined by bulk major element oxide characteristics. From the modal composition of QFL components, the sands can be classified predominantly as litharenites with the lithic component characterized by both rhyolitic and basaltic grains (rhyolitic lithics are however dominant). Bulk major oxide characteristics are also consistent with the sands being produced in an arid (to semi-arid) environments with CIAs indices ranging from 50 to 65. Both bulk major element oxide and bulk trace element compositions (specifically the rare earth elements) are broadly consistent with derivation from (a) felsic igneous province(s) and exhibit geochemical characteristics of Earth's bulk upper continental crust (e.g. Dy_N/Lu_N from 1.2 to 1.4). When compared to regional dune systems throughout the western US the Tonopah sands are compositionally similar to the dune fields across the central Mojave Desert, in particular the Cadiz, Danby, and Daly Lake sands of eastern California. They are however distinct from the dune fields of the Parker dunes of Arizona and the Algodones dunes (also California) where an origin from Colorado River sediments has previously been established. Similar bulk elemental compositions to central Mojave desert dune systems is therefore consistent with the derivation of the Tonopah sands from chemically evolved (igneous) provinces. The derivation and provenance of the Tonopah sands was further evaluated by comparing bulk major element compositions to

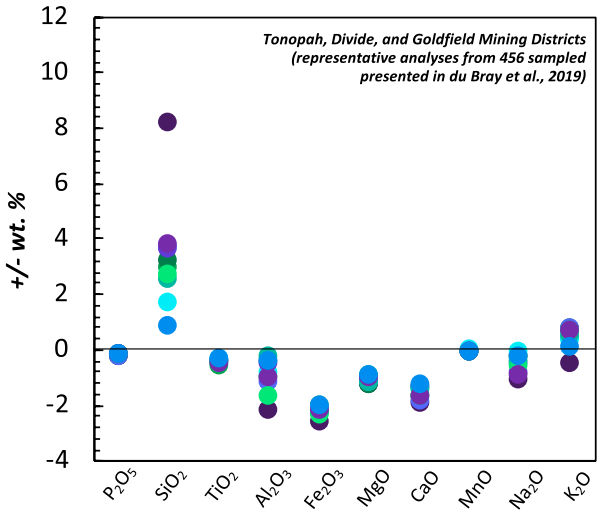

Fig. 13. Comparison of bulk elemental characteristics of Tonopah sand to the bulk composition of volcanic rock suites in and around Tonopah (reported in du Bray et al. 2019).

regional and local bedrock compositions, including a recently compiled dataset for the chemically evolved Miocene-aged andesites-dacites-rhyolites across Tonopah and mining districts to the south. Compared to the regional bedrock (Nye County), local bedrock (Tonopah), and the Miocene-aged volcanics, the Tonopah sands are consistently enriched in wt% SiO_2 and Al_2O_3 (and to a lesser extent K_2O and Na_2O), and relatively depleted in wt% MgO and CaO. This is consistent with the quartzofeldspathic nature of the sands and the likely secondary process of wind action promoting the development of quartz-rich sands. When compared to these regional and local compositions, the argument can be made that the Tonopah sands are the most similar (when all chemical components and potential sources are considered) to the Miocene-aged volcanics however this could be further investigated (and constrained) via future geochronological study of the accessory phase components of the sands (e.g. U-Pb in zircon).

This comprehensive study provides mineralogical, geochemical and context for future environmental studies in the region including sand and dust provenance, soil science, mine waste pollution, and studies of environmental change. In particular, the Pb concentrations and reflective spectroscopy data serve as important references for specific environmental study. This investigation has demonstrated the multidisciplinary utility of dune sands in Nevada for establishing environmental contexts for a region that is in high need of environmental study and action.

Declaration of Competing Interest

The authors declare that they have no known competing financial interests or personal relationships that could have appeared to influence the work reported in this paper.

Acknowledgements

We thank Matt Duley and Dr. Richard Edelmann at the Center for Advanced Microscopy and Imaging at Miami University for assistance with SEM-EDS data collection. Field work and sample collection was supported by a NSF GEOPATHS-EXTRA award to McLeod and Krekeler (#1801424). Additional thanks are extended to Daniel Blakemore for assistance during sample preparation and Miami University Regional Campus Deans office who provided partial student support to Oglesbee. We thank two anonymous reviewers and the editor for providing constructive and comprehensive guidance throughout the review process. Their feedback contributed significantly to enhancing the scope of this work.

Appendix A. Supplementary material

Supplementary data to this article can be found online at https://doi.org/10.1016/j.catena.2020.104640.

References

Adhikari, A.R., Acharya, K., Shanahan, S.A., Zhou, X., 2011. Removal of nutrients and metals by constructed and naturally created wetlands in the Las Vegas Valley, Nevada. Environ. Monit. Assess. 180, 97–113.

Agency for Toxic Substances and Disease Registry (ATSDR), 2019. Toxicological profile for Lead. (Draft for Public Comment). U.S. Department of Health and Human Services, Public Health Service, Atlanta, GA.

Allen, C.S., Krekeler, M.P.S., 2011. Crude oil, petroleum and water discrimination on terrestrial substrates with airborne imaging spectroscopy. In: Proc. of SPIE Active and Passive Signatures 8040, 80400L International Society for Optics and Photonics.

Aumann, H.H., Gregorich, D., Gaiser, S., 2005. AIRS hyper-spectral measurements for climate research: Carbon dioxide and nitrous oxide effects. Geophys. Res. Lett. 32, L05806.

Barnes, M., McLeod, C., Faraci, O., Chappell, C., Krekeler, M.P.S., 2020. Characterizing the geogenic background of the Midwest: A detailed mineralogical and geochemical investigation of a glacial till in southwestern Ohio. Environ. Earth. Sci. 79, 159.

Bastin, E.S. 1922. Bonanza Ores of the Comstock Lode, Virginia City, Nevada. Contributions to Economic Geology Part 1, USGS report. Available online at: https://pubs.usgs.gov/bul/0735c/report.pdf.

Bishop, C.A., Liu, J.G., Mason, P.J., 2011. Hyperspectral remote sensing for mineral exploration in Pulang, Yunnan Province, China. Int. J. Remote Sens. 32, 2409–2426.

Carlson, K.M., Asner, G.P., Hughes, R.F., Ostertag, R., Martin, R.E., 2007. Hyperspectral remote sensing of canopy biodiversity in Hawaiian lowland rainforests. Ecosystems 10, 536–549.

Choe, E., van der Meer, F., van Ruitenbeek, H., van der Werff, B., de Smeth, W., Kim, K.-W., 2008. Mapping of heavy metal pollution in stream sediments using combined geochemistry, field spectroscopy, and hyperspectral remote sensing: A case study of the Rodalquilar mining area, SE Spain. Remote Sens. Environ. 112, 3222–3233.

Cizdziel, J., Hinners, T., Cross, C., Pollarda, J., 2003. Distribution of mercury in the tissues of five species of freshwater fish from Lake Mead, USA. The Royal Soc. Chem. 802–807.

Cracknell, M.J., Reading, A.M., 2014. Geological mapping using remote sensing data: A comparison of five machine learning algorithms, their response to variations in the spatial distribution of training data and the use of explicit spatial information. Comput. Geosci. 63, 22–33.

Crouvi, O., Ben-Dor, E., Beyth, M., Avigad, D., Amit, R., 2006. Quantitative mapping of arid alluvial fan surfaces using field spectrometer and hyperspectral remote sensing. Remote Sens. Environ. 104, 103–117.

Custer, C.M., Custer, T.W., Hill, E.F., 2007. Mercury Exposure and Effects on Cavity-Nesting Birds from the Carson River, Nevada. Arch. Environ. Contam. Toxicol. 52, 129–136.

Davies, G.E., Calvin, W.M., 2017. Mapping acidic mine waste with seasonal airborne hyperspectral imagery at varying spatial scales. Environ. Earth Sci. 76, 432.

Dickinson, W.R., Beard, L.S., Brakenridge, G.R., Erjavec, J.L., Ferguson, R.C., Inman, K.F., Knepp, R.A., Lindberg, F.A., Ryberg, P.T., 1983. Provenance of North American Phanerozoic sandstones in relation to tectonic setting. GSA Bull. 94, 222–235.

Donato, D.B., Nichols, O., Possingham, H., Moore, M., Ricci, P.F., Noller, B.N., 2007. A critical review of the effects of gold cyanide-bearing tailings solutions on wildlife. Environ. Int. 33, 974–984.

du Bray, E.A., John, D.A., Colgan, J.P., Vikre, P.G., Cosca, M.A., Morgan, L.E., 2019, Petrology of volcanic rocks associated with silver-gold (Ag-Au) epithermal deposits in the Tonopah, Divide, and Goldfield mining districts, Nevada: U.S. Geological Survey Scientific Investigations Report 2019–5024, 22 p., https://doi.gov/10.3133/sir20195024.

Eckley, C.S., Gustin, M., Marsik, F., Miller, M.B., 2011. Measurement of surface mercury fluxes at active industrial gold mines in Nevada (USA). Sci. Tot. Environ. 409, 514–522.

Engle, M.A., Gustin, M.S., Zhang, H., 2001. Quantifying natural source mercury emissions from the Ivanhoe Mining District, north-central Nevada, USA. Atmos. Environ 35, 3987–3997.

Goldberg, K., Humayun, M., 2010. The applicability of the Chemical Index of Alteration as a paleoclimatic indicator: An example from the Permian of Paraná Basin, Brazil. Palaeogeogr., Palaeoclimatol., Palaeoecol. 293, 175–183.

Goossens, D., Buck, B.J., Teng, Y., McLaurin, B.T., 2015. Surface and Airborne Arsenic Concentrations in a Recreational Site near Las Vegas, Nevada, USA. PLOSONE|DOI:10.1371/journal.pone.0124271.

Goossens, D., Buck, B., 2010. Gross erosion, net erosion and gross deposition of dust by wind: field data from 17 desert surfaces. Earth Surf. Process. Land. 36, 610–623. https://doi.org/10.1002/esp.2080.

Goossens, D., Buck, B., McLaurin, B., 2012. Contribiutions to atmospheric dust prodcution of natural and anthropogenic emissions in a recreational area designated for off-road vehicular activity (Nellis Dunes, Nevada, USA). J. Arid Environ. 78, 80–99.

Gostin, L.O., 2016. Lead in the water: a tale of social and environmental injustice. JAMA. J. Am. Med. Assoc. 315, 2053–2054.

Grandjean, P., 2010. Even low-dose lead exposure is hazardous. Lancet 376, 855–856.

Grandjean, P., Landrigan, P.J., 2014. Neurobehavioural effects of developmental toxicity. Lancet Neurol. 13, 330–338.

Henny, C.J., Hill, E.F., Hoffman, D.J., Spalding, M.G., Grove, R.A., 2002. Nineteenth

century mercury: hazard to wading birds and cormorants of the Carson River, Nevada. Ecotoxicology 11, 213–231.
Heyvaert, A.C., Reuter, J.E., Slotton, D.G., Goldman, C.R., 2000. Paleolimnological reconstruction of historical atmospheric lead and mercury deposition at Lake Tahoe, California – Nevada. Environ. Sci. Technol. 34, 3588–3597.
Hörig, B., Kühn, F., Oschütz, F., Lehmann, F., 2001. HyMap hyperspectral remote sensing to detect hydrocarbons. Int. J. Remote Sens. 22, 1413–1422.
Huang, J.H., Liu, W.C., Zeng, G.M., Li, F., Huang, X.L., Gu, Y.L., Shi, L.X., Shi, Y.H., Wan, J., 2016. An exploration of spatial human health risk assessment of soil toxic metals under different land uses using sequential indicator simulation. Ecotoxicol. Environ. Saf. 129, 199–209.
Hugenholtz, C.H., Levin, N., Barchyn, T.E., Baddock, M.C., 2012. Remote sensing and spatial analysis of aeolian sand dunes: A review and outlook. Earth. Sci. Rev. 111, 319–334.
Hunt, G., Salisbury, J.W., Lenhoff, C.J., 1971. Visible and Near-infrared Spectra of Minerals and Rocks: III. Oxides and Hydroxides". Modern Geol. 2, 195–205.
Hunt, G., Salisbury, J.W., Lenhoff, C.J., 1973. Visible and Near Infrared Spectra of Minerals and Rocks.: VI. Additional silicates. Modern Geol. 4, 85–106.
Jarup, L., 2003. Hazards of heavy metal contamination. Brit. Med. Bull. 68, 167–182.
Kasper-Zubillaga, J.J., Zolezzi-Ruiz, H., 2007. Grain size, mineralogical and geochemical studies of coastal and inland dune sands from El Vizcaíno Desert, Baja California Peninsula, Mexico. Revista Mexicana de Ciencias Geológicas 24, 423–438.
Keila, D.E., Buck, B., Goossens, D., McLaurin, B., Murphy, L., Leetham-Spencera, M., Teng, Y., Pollard, J., Gerards, R., DeWitt, J.C., 2018. Nevada desert dust with heavy metals suppresses IgM antibody production. Toxicol. Rep. 5, 258–269.
Kersting, A.B., Efurd, D.W., Finnegan, D.L., Rokop, D.J., Smith, D.K., Thompson, J.L., 1999. Migration of plutonium in ground water at the Nevada Test Site. Nature 397, 56–59.
Ko, S., Schaefer, P.D., Vicario, C.M., Binns, H.J., 2007. Relationships of video assessments of touching and mouthing behaviors during outdoor play in urban residential yards to parental perceptions of child behaviors and blood lead levels. J. Expo. Sci. Epidemiol. 17, 47–57.
Kocurek, G., Lancaster, N., 1999. Aeolian sediment state: theory and Mojave Desert Kelso Dune field example. Sedimentology 46, 505–515.
Krekeler, M.P.S., Allen, C.S., 2008. Allen, Remote sensing spectra of cesium chloride provide a potential emergency management tool for response to a radiological dispersal device detonation. J. Emerg. Manage. 6. https://doi.org/10.5055/jem.2008.0014.
Kruse, F.A., Boardman, J.W., Huntington, J.F., 2003. Comparison of airborne hyperspectral data and EO-1Hyperion for mineral mapping. IEEE Trans. Geosci. Remote Sens. 41, 1388–1400.
Lanphear, B.P., Hornung, R., Khoury, J., Yolton, K., Baghurst, P., Bellinger, D.C., Canfield, R.L., Dietrich, K.N., Bornschein, R., Greene, T., Rothenberg, S.J., 2005. Low-level environmental lead exposure and children's intellectual function: an international pooled analysis. Environ. Health Perspect. 1, 894–899.
Lancaster, N., 2013. Sand seas and dune fields. In: Shroder, J.F., Editor-in-Chief, Treatise on Geomorphology. Academic Press, San Diego; 219-245.
Lancaster, N., Baker, S., Bacon, S., McCarley-Holder, G., 2015. Owens Lake dune fields: Composition, sources of sand, and transport pathways. Catena 134, 41–49.
Leblanc, G., Francis, C.M., Soffer, R., de Kalacska, M., Gea, J., 2016. Spectral reflectance of polar bear and other large arctic mammal pelts; potential applications to remote sensing surveys. Remote Sens. 8, 273.
LeGalley, E., Widom, E., Krekeler, M.P.S., Kuentz, D.C., 2013. Chemical and lead isotope constraints on sources of metal pollution in street sediment and lichens in southwest Ohio. Appl. Geochem. 32, 195–203.
Leifer, I., Lehr, W.J., Simecek-Beatty, D.E., Bradley, R., Clark, P., Dennison, Y., Hu, S., Matheson, C.E., Jones, B., Holt, M., Reif, D.A., Roberts, J., Svejkovsky, G., Swayze, J., Wozencraft, J., 2012. State of the art satellite and airborne marine oil spill remote sensing: Application to the BP *Deepwater Horizon* oil spill. Remote Sens. Environ. 124, 185–209.
Mars, J.C., Crowley, J.K., 2003. Mapping mine wastes and analyzing areas affected by selenium-rich water runoff in southeast Idaho using AVIRIS imagery and digital elevation data. Remote Sens. Environ. 84, 422–436.
McKenna Neuman, C., Lancaster, N., Nickling, W.G., 1997. Relations between dune morphology, air flow, and sediment flux on reversing dunes, Silver Peak, Nevada. Sedimentology 44, 1103–1113.
McLaurin, B.T., Goossens, D., Buck, B.J., 2011. Combining surface mapping and process data to assess, predict, and manage dust emissions from natural and disturbed land surfaces. Geosphere 7, 260–275. https://doi.org/10.1130/GES00593.1.
Miller, J.R., Rowland, J., Lechler, P.J., Desilets, M., Hsu, L.C., 1996. Dispersal of Mercury-Contaminated Sediments by Geomorphic Processes, Sixmile Canyon, Nevada, USA: Implications to Site Characterization and Remediation of Fluvial Environments. Water Air Soil Poll. 86, 373–388.
Miller, J.R., Lechler, P.J., Desilets, M., 1998. The role of geomorphic processes in the transport and fate of mercury in the Carson River basin, west-central Nevada. Environ. Geol. 33, 249–262.
Muhs, D.R., Reynolds, R.R., Been, J., Skipp, G., 2003. Eolian sand transport pathways in the southwestern United States: importance of the Colorado River and local sources. Quat Int. 104, 3–18.
Muhs, D.R., 2004. Mineralogical maturity in dunefields of North America, Africa and Australia. Geomorphology. 59, 247–269.
Muhs, D.R., 2017. Evaluation of simple geochemical indicators of aeolian sand provenance: Late Quaternary dune fields of North America revisited. Quat. Sci. Rev. 171, 260–296.
Muhs, D.R., Bush, C.A., Cowherd, S.D., Mahan, S., 1995. Geomorphic and geochemical evidence for the source of sand in the Algodones dunes, Colorado desert, southeastern California. In: Tchakerian, V.P. (Ed.), Desert Aeolian Processes. Springer, Dordrecht.
Muhs, D.R., Lancaster, N., Skipp, G.L., 2017. A complex origin for the Kelso Dunes, Mojave National Preserve, California, USA: A case study using a simple geochemical method with global applications. Geomorph. 276, 222–243.
NCMR, 2017. Major Mines of Nevada 2017. Accessed online December 2019. Available at: http://minerals.nv.gov/uploadedFiles/mineralsnvgov/content/Programs/Mining/MiningForms/mm2017_Major_Mines_all.pdf.
Needleman, H., 2004. Lead poisoning. Annu. Rev. Med. 55, 209–222.
Nesbit, H.W., Young, G., 1982. Early Proterozoic climate and plate motions inferred from major chemistry of lutites. Nature 279, 715–717.
Nickling, W.G., McKenna, C., Lancaster, N., 2002. Grainfall processes in the lee of traverse dunes, Silver Peak, Nevada. Sedimentology 49, 191–209.
Nye County, 2018. Nye County Brownfields Program. https://www.nyecounty.net/647/Nye-County-Brownfields-Program.
Powers, M.C., 1953. A new roundness scale for sedimentary particles. J. Sedimentary Res. 23, 117–119.
Pepe, N.E., 2014. The Geomorphology, Eolian Activity, and Petrology of the Winnemucca Dune Complex, Humboldt County, Nevada, Geological Sciences. University of Nevada, Reno, Reno, NV, PhD thesis. [Accessed 03.22.20].
Perry, R., Visher, M., 2015. Major Mines of Nevada 2014. Nevada Division of Minerals, Reno, NV. Nevada Bureau of Mines and Geology Special Publication P-26. Available online at: http://minerals.nv.gov/uploadedFiles/mineralsnvgov/content/Programs/Mining/Forms_Publications/mm2014_MajorMines2014_9Oct15.pdf.
Pettijohn, F.J., Potter, P.E., Siever, R., 1973. Sand and Sandstone. Springer-Verlag, New York, pp. 618.
Rudnick, R.L, Gao, S., 2003. Composition of the Continental Crust. Treatise on Geochemistry, 3, (eds), Holland, H.D, Turekian, K.K, pp. 659, p. 1-64.
Sabins, F.F., 1999. Remote sensing for mineral exploration. Ore Geol. Rev. 14, 157–183.
Seibert, Z., McLeod, C., Blakemore, D., Krekeler, M.P.S., 2019. Volcanism Associated with Crustal Extension in the Basin and Range Province. Geological Society of America Abstracts with Programs, 51, 5. Available online at: 10.1130/abs/2019AM-340873.
Sheppard, P.R., Speakman, R.J., Ridenour, G., Witten, M.L., 2007. Temporal Variability of Tungsten and Cobalt in Fallon, Nevada. Environ. Health Persp. 115, 715–719.
Sheppard, P.R., Helsel, D.R., Speakman, R.J., Ridenour, G., Witten, M.L., 2012. Additional analysis of dendrochemical data of Fallon. Nevada. Chemico-Biolog. Interact. 196, 96–101.
Sims, D.B., 2010. Contaminant Mobilization from Anthropogenic Influences in the Techatticup Wash, Nelson, Nevada (USA). Soil Sed. Contam. 19, 515–530.
Sims, D.B., Hooda, P.S., Gilmore, G.K., 2013. Sediment Contamination along Desert Wash Systems from Historic Mining Sites in a Hyperarid Region of Southern Nevada, USA. Soil Sed. Contam. 22, 737–752.
Soukup, D., Buck, B., Goossens, D., Ulery, A., McLaurin, B.T., Baron, D., Teng, Y., 2012. Arsenic concentrations in dust emissions from wind erosion and off-road vehicles in the Nellis Dunes Recreational Area, Nevada, USA. Aeolian Res. 5, 77–89.
Streckeisen, A.L., 1976. Classification of the common igneous rocks by means of their chemical composition: a provisional attempt: Neues Jahrbur För Mineralogie. Monatshefte H.1, 1–15.
Streckeisen, A.L., 1978. IUGS Subcommission on the Systematics of Igneous rocks. Classification and Nomenclature of Volcanic Rocks, Lamprophyres, Carbonatites and Melilite rocks. Recommendations and Suggestions: Neues Jahrbuch FörMineralogie, Abhandlungen 141, 1–14.
Stewart, L.R., Farver, J.R., Gorsevski, P.V., Miner, J.G., 2014. Spatial prediction of blood lead levels in children in Toledo, OH using fuzzy sets and the site-specific IEUBK model. Appl. Geochem. 45, 120–129.
Swayze, G.A., Smith, K.S., Clark, R.N., Sutley, S.J., Pearson, R.M., Vance, J.S., Hageman, P.L., Briggs, P.H., Meier, A.L., Singleton, M.J., Roth, S., 2000. Using imaging spectroscopy to map acidic mine waste. Environ. Sci. Tech. 34, 47–54.
USGS (United States Geological Survey) 2014. Mineral Commodity Summaries. Available online at: https://www.usgs.gov/centers/nmic/mineral-commodity-summaries [Accessed 18 December 2019].
Ustin, S.L., DiPietro, D., Olmstead, K., Underwood, E., Scheer, G.J. 2002. Hyperspectral remote sensing for invasive species detection and mapping. In Geoscience and Remote Sensing Symposium, IGARSS'02. 2002 IEEE International 3:1658-1660.
Ustin, S.L., Valko, P.G., Kefauver, S.C., Santos, M.J., Zimpfer, J.F., Smith, S.D., 2009. Remote sensing of biological soil crust under simulated climate change manipulations in the Mojave Desert. Remote Sens. Environ. 113, 317–328.
Walker, I.J., 1999. Secondary airflow and sediment transport in the Lee of a reversing dune. Earth Surf. Process. Land. 24, 437–448.
Yang, Z.R., Graham, E.Y., Lyons, W.B., 2003. Geochemistry of Pyramid Lake sediments: influence of anthropogenic activities and climatic variations within the basin. Environ. Geol. 43, 688–697.
Zimbelman, J.R., Williams, S.H., 2002. Geochemical indicators of separate sources for eolian sands in the eastern Mojave Desert, California, and western Arizona. GSA Bull. 114, 490–496.